Materials Today Energy 22 (2021) 100852

Contents lists available at ScienceDirect

Materials Today Energy

journal homepage: www.journals.elsevier.com/materials-today-energy/

A review on semitransparent solar cells for agricultural application

Yepin Zhao [a], Yuan Zhu [a], Hao-Wen Cheng, Ran Zheng, Dong Meng, Yang Yang*

Department of Materials Science and Engineering and California Nano Systems Institute, University of California, Los Angeles, CA, 90095, United States

ARTICLE INFO

Article history:
Received 12 July 2021
Received in revised form
31 August 2021
Accepted 31 August 2021
Available online 15 September 2021

Keywords:
Organic photovoltaics
Photosynthesis
Active layer
Electrode
Power conversion efficiency
Transmittance
Greenhouse

ABSTRACT

Modern agriculture dramatically increases food production and continuously plays a critical role to remit the food crisis in the world. However, agricultural modernization also consumes more energy and land than the traditional small-scale peasant farming. The integration of photovoltaics into modern agriculture is a promising method to utilize the vast agricultural land efficiently and provide extra energy for crop production. Due to the tunable energy of the organic molecules, semitransparent organic solar cell serves as an ideal candidate. Rationally designed devices can allow sunlight with selected wavelengths to pass though and get absorbed by the plants for photosynthesis. Meanwhile, relatively high photovoltaic performances are also preferred for energy generation. In this article, important studies of semitransparent organic solar cells for agricultural applications are reviewed, and the design routes and strategies are summarized. The perspectives for the future research on agricultural photovoltaics are also presented.

1. Introduction

As the global population continues to grow, combined with global warming and water scarcity, it is imperative to develop technologies that can increase annual crop yield and yield stability from sustainable agriculture [1]. The installation of greenhouses, in which the inner conditions such as temperature, moisture, and sun-light level are finely controlled, makes it possible to prolong the cultivation season and broaden the crop species, no matter what the outdoor weather is [2,3]. However, greenhouse operation comes with large energy consumption on heating, cooling, artificial lighting, pumping and ventilation, resulting in unwanted environmental effects. Hence it will be desirable to create a 'self-powered' system within the greenhouse to offset its own energy consumption (Fig. 1a). People conceive of building photovoltaic (PV) greenhouse by integrating PV panels onto the greenhouse's walls and roofs. The shared structure of PV greenhouses leads to many benefits, including clean electricity generation, reduced installation material costs and rational use of valuable land resources [4–6].

Greenhouse layout design is both climate and crops specific. Several literatures have given detailed descriptions about the structures, facilities, and categories of various greenhouses [7–9]. Basically, a greenhouse is constituted of a metal framework covered with transparent claddings made of either plastics or glasses, and they should be mechanically strong enough to physically protect crops from harsh weather (Fig. 1b). The main goal of greenhouses is to create an enclosed and controlled microclimate for all-year-round and high-quality crop productions. The shared structure of PV modules-integrated greenhouse allows electricity to be closely sourced and helps to save precious land resources (Fig. 1c). There are multiple ways to integrate PV modules onto greenhouses. Historically, opaque crystalline silicon and other thin film PVs are mounted to greenhouse roofs [10–15]. In this fashion, the inclination of flaps on greenhouse roofs lets sun rays reach the PV panels with suitable incident angles. In addition, the opaque PV modules can also act as partial shadings, avoiding over-heating of the greenhouse and lowering the cooling loads during hot summer session [8]. However, the competition between the mounted PV modules and the crops results in decreased crop yields, and thus this method was not widely adopted [16,17]. A slight modification of this method is to use Fresnel lenses embedded to the greenhouse roofs. In this way, direct sunlight will be used for photovoltaic generation, while diffuse sunlight is allowed to penetrate deeply through the greenhouse for crop growth (Fig. 1d). Unfortunately, this method often requires costly and complex tracking equipment [18]. Mounting semitransparent PV modules onto both the roofs and walls of greenhouses is the third way, by which lights with wavelengths that are favorites of plant species can pass through for

* Corresponding author.
E-mail address: yangy@ucla.edu (Y. Yang).
[a] These authors contributed equally to this work.

https://doi.org/10.1016/j.mtener.2021.100852
2468-6069/

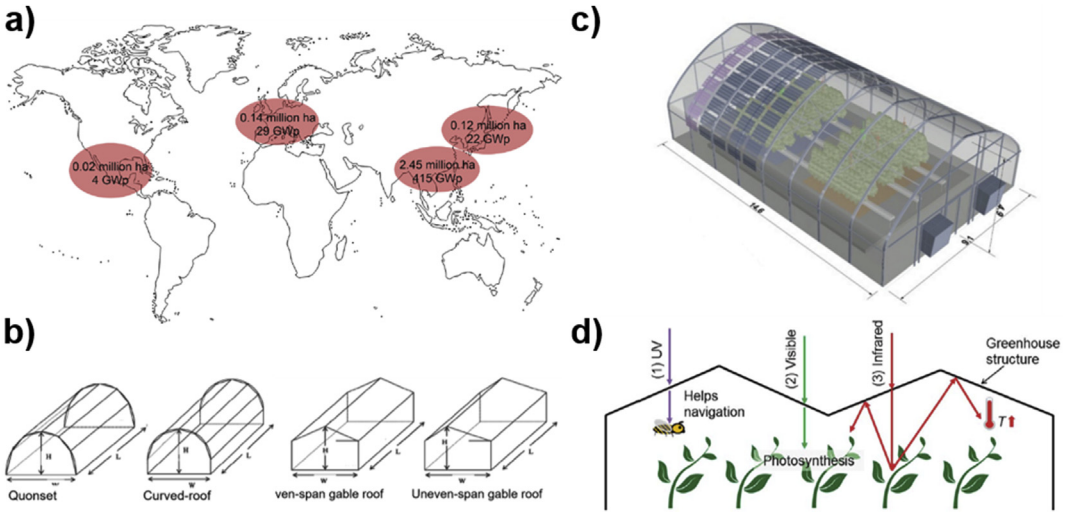

Fig. 1. Global electricity generating capacity and prototypes of greenhouses. (a) Potential solar electricity generating capacity of the worldwide greenhouse area. (b) Main types of greenhouses. (c) 3-D schematic of the greenhouse integrated with PVs. (d) Cartoon of the effect of light on greenhouse crop production. Reproduced (a, d) with permission from ref. [18], (b) with permission from ref. [8], and (c) with permission from ref. [3]. Copyright 2015 The Royal Society of Chemistry, 2021 MPDI, and 2020 Elsevier, respectively.

crop growth, whereas the remainder portions are harnessed by photovoltaics for electricity generation. Ideally, this method allows maximum utilization of solar radiation while keeping the implementation process simple. However, it is still challenging for semitransparent PV modules to absorb solar spectrum selectively. Thanks to organic semiconductors, whose bandgaps can be readily tuned by manipulating the molecular structures, semitransparent PV modules that are suitable for greenhouse applications can be realized.

Semitransparent organic photovoltaics (OPV) are promising candidates to be integrated to greenhouses for electricity generation and have limited impact on crop growth. The recent discovery of non-fullerene organic small molecule acceptors has pushed the opaque solar cell's power conversion efficiency to 18%, which is close to the commercialization level [19–24]. In addition, the power conversion efficiency (PCE) of semitransparent OPV has also reached over 13% with a relatively high averaged visible light transmittance (over 20%). Compared to inorganic photovoltaics, OPVs also have many of their own unique advantages. The solution processability of OPVs indicates that the devices can be subjected to roll-to-roll printing for large-area depositions under large scale manufacture [25,26]. In addition, the lightweight OPVs can be deposited onto flexible substrates, and the substrate materials can be very similar to low density polyethylene, the most used plastics for greenhouse claddings [18]. As a result, expenses of materials for either building new PV greenhouses or retrofitting the old ones with OPVs-covered walls and roofs will become acceptable. Finally, the non-toxic nature of the selected OPV materials for greenhouse applications protects clean soil and water resources that are indispensable for safe and healthy crop growth. However, as mentioned, due to the overlap of the absorption spectra of the semitransparent devices and the plants in the greenhouses, the application of the solar cells might bring negative effects to the photosynthesis process, which may slow down the growth rate and quality of the plants.

In the review, we summarize current research on semitransparent OPVs for agricultural application. Different from the other applications of the semitransparent OPVs such as building integration or wearable electronics, we will introduce the special requirements of OPVs for agricultural application, and relative computational evaluations of OPV integrated greenhouses. Learning from the experiences of normal semitransparent OPV development, we provide the strategies demonstrated so far for the enhancement of the photovoltaic performances and the transparency of the OPVs for agricultural application. The strategies are divided into three categories: active layer material designs, electrode developments, and structural modifications. Finally, we provide our guidance and perspectives on agricultural photovoltaics in the future.

2. Special requirements of OPVs for agricultural application

A functional design of semitransparent OPV greenhouses requires a thorough understanding about how solar radiation affects both crop growth and photovoltaics' electricity generation efficiency and the balance between them. Plant photosynthesis mainly requires sunlight within the visible spectrum (400–700 nm), named photosynthetically active radiation (PAR), but not all wavelengths will be absorbed by crops equally. Typically, there are absorption peaks of photosynthesis rate within the red-orange and blue region, with a minimum demand on green light due to chlorophyll's poor absorption [27]. Near infrared (NIR) light, which makes up around 50% of solar spectrum, contributes little to plant growth [28], so it becomes the most suitable bandwidth for photovoltaics to extract energy from. There are two ways to quantify the influences of solar panel implementations on crop growth. The most widely used parameter indicating semitransparent OPV's transmittance in literatures is average visible transmittance (AVT), which is the weighted transmission spectrum of semitransparent OPVs against the photopic response of the human eyes [3]. However, it is more reasonable to have an index that can directly reflect the impact of semitransparent OPV integrated onto the greenhouse on crop growth, and crop growth factor (G) satisfies the need. The crop growth factor G(x) as a function of active layer thickness is defined as following:

$$G(x) = \frac{\int T(x,\lambda) b_s(\lambda) a(\lambda) d\lambda}{\int b_s(\lambda) a(\lambda) d\lambda}$$

where $T(x,\lambda)$ indicates the active layer thickness- and light wavelength-dependent transmission of the semitransparent OPV,

and $b_s(\lambda)a(\lambda)$ represents the photon flux density required for optimizing plant growth. In a nutshell, $G(x)$ is the ratio between the crop's photosynthesis rate under greenhouse materials and the rate under a clear sky, and the growth of the greenhouse crops is decreased for 1% for every 1% reduction in photosynthesis rate.

3. Computational evaluations of OPV integrated greenhouses

Computer modeling plays an important role in evaluating the performance of semitransparent OPV integrated greenhouses due to its fast and massive data processing of the sophisticated sharing system of power generation and living creature growth. Recently, researchers have developed specific models to address certain problems associated with material selection, shading effects, and crop-oriented set up on semitransparent OPV integrated greenhouses. First, materials used within the active layer of semitransparent OPVs are one of the paramount parameters that should be investigated for functional PV modules' design. Therefore, Emmott and coworkers apply transfer matrix optical modeling to assess the efficiency and spectrally resolved transparency of five different polymer donors with large, middle and narrow bandgaps, blended with two common fullerene acceptors 6,6-phenyl C61-butyric acid methyl ester (PCBM) and 6,6-phenyl C71-butyric acid methyl ester ($PC_{70}BM$) [18]. As a result, they plot crop growth factor, G, against current and PCE of semitransparent OPV modules. It is figured out that although low-band-gap polymers show larger NIR absorption and high PAR, they might not always overperform large-band-gap polymers because large-band-gap polymers' higher PCE can compensate for their lower PAR. Compared to PCBM, $PC_{70}BM$ is employed to broaden absorption that cannot be achieved by typical polymer donors to achieve higher overall PCEs' percentage. Unfortunately, $PC_{70}BM$ is less suitable than PCBM for greenhouse applications because the former has too much absorption within the PAR region. Emmott and coworkers are the first to optimize spectral absorbance to enable crop growth through modeling, and their research result signifies that when selecting materials for semitransparent OPV in greenhouse applications, both influences of device efficiency and transparency on crop growth should be considered carefully.

Some other research works focus on the overall operational performance of semitransparent OPV integrated greenhouses by simultaneously simulating the greenhouse's working load and power generation of semitransparent OPV panels. Ravishankar et al. introduce a tailored energy balance model to predict whether the power generation can meet the energy consumption demand to achieve 'Net Zero Energy' greenhouses (Fig. 2a) [29]. In their research, they develop a detailed dynamic energy balance model that uses mass and energy balances to mimic the inner environment (temperature, humidity, etc.) and accurately describe the incident solar insolation onto the greenhouse surfaces. Their model also reflects any load change of the greenhouse after the PV panels are employed. By comparing the calculated load with the power produced by semitransparent OPVs predicted by the optical model for different geographical locations, they conclude that 'Net Zero Energy' greenhouses can be realized in warm and hot regions, while they are impossible in cold climate.

Computer modeling was also used for more specific aspects of semitransparent OPV integrated greenhouses, and the simulated results become references for future greenhouses design. For example, Baxevanou et al. apply computational fluid dynamics using the discrete ordinates model to simulate the radiation transmission through the PV cover and into the greenhouses, the emitted thermal radiation, and the radiation transport within the designated area to investigate the shading effects of different densities of semitransparent OPV modules (Fig. 2b) [30]. They conclude that only certain combinations of thicknesses and densities of semitransparent OPV/PE films (substrate) can meet the PAR threshold requirement. Waller and coworkers combine computer modeling and realistic semitransparent OPV-integrated greenhouses set-up to research the shading effects of semitransparent OPV modules, and they demonstrate the feasibility of using semitransparent OPV modules as shadings for high light condition during spring and summer session [3]. The modeling of the effects of semitransparent OPV modules can also be crop species-specific. For example, Tang et al. start specific modeling for strawberry production in a semitransparent OPV integrated greenhouse (Fig. 2c) [31]. In the future, further modeling should test the light requirement of multiple types of crops, seasonal effects of semitransparent OPV modules, influences of semitransparent OPV modules on water and nutrition of crops, spectral degradation of semitransparent OPV modules, and other meaningful factors that affect semitransparent OPV efficiencies and crop growth.

4. Current methods and strategies of the OPV design for agricultural application

4.1. Active layer material design

Different from the traditional opaque organic solar cells, the semitransparent solar cells, especially the ones for agricultural application, require high transmittance in the visible wavelength region. Hence, materials with high absorption in near infrared (NIR) and ultraviolet (UV) region are highly demanded. Besides that, we need to ensure that the PCE of the device will not be lowered too much because of the reduced photon utilization, since efficient carrier dissociation and transportation are also required. In this section, we start from the active layers of normal semitransparent OPVs and summarize the design routines for high performance and high AVT devices. Then we will further discuss the special requirements of the devices for the greenhouse application. The corresponding strategies and device performances are summarized in Table 1.

4.1.1. NIR absorbing donors/acceptors

To meet the requirements of high AVT, one basic design routine is to use NIR absorbing materials for the active layer to reduce or avoid the absorption within the visible wavelength range [32–36]. Forrest et al. demonstrated a semitransparent OPV with PCE of 10.8 ± 0.5% and AVT of 45.7 ± 2.1% by incorporating a NIR absorbing and partly fused non-fullerene acceptor (NFA)-based donor/acceptor into a bulk heterojunction (Fig. 3a) [35]. They compared the fully fused NFA, SBT-FI, with two of its partly fused isomers, A078 and A134, each containing one benzene ring, two cyclopentadienes, and four thiophenes. When supplied an additive to these partially fused rigid NFAs, contrary to the expectations, it was observed that NIR absorption became stronger and molecular packing were closer. This counterintuitive phenomenon resulted from the central IDT unit and the S···S interaction between the 2-ethylhexanethiol group planarizing and rigidifying the π-conjugated molecules. Therefore, the partly fused NFAs aggregate led to a reduced bandgap (E_g) with absorption peak at $\lambda > 900$ nm. Also, employing a PN additive enhanced the intermolecular π–π interactions within the partly fused NFAs, contributing to an increased J_{SC} and *FF*.

Hou et al. also designed and synthesized a new non-fullerene acceptor named IEICO-4Cl via chlorination [36]. IEICO-4Cl has a narrow bandgap of 1.23 eV with weak absorption in the visible region. The IEICO-4Cl-based blend films could easily change color from purple, blue to cyan when J52, PBDB-T, and PTB7-Th were used as polymer donors, respectively. The semitransparent OPVs with

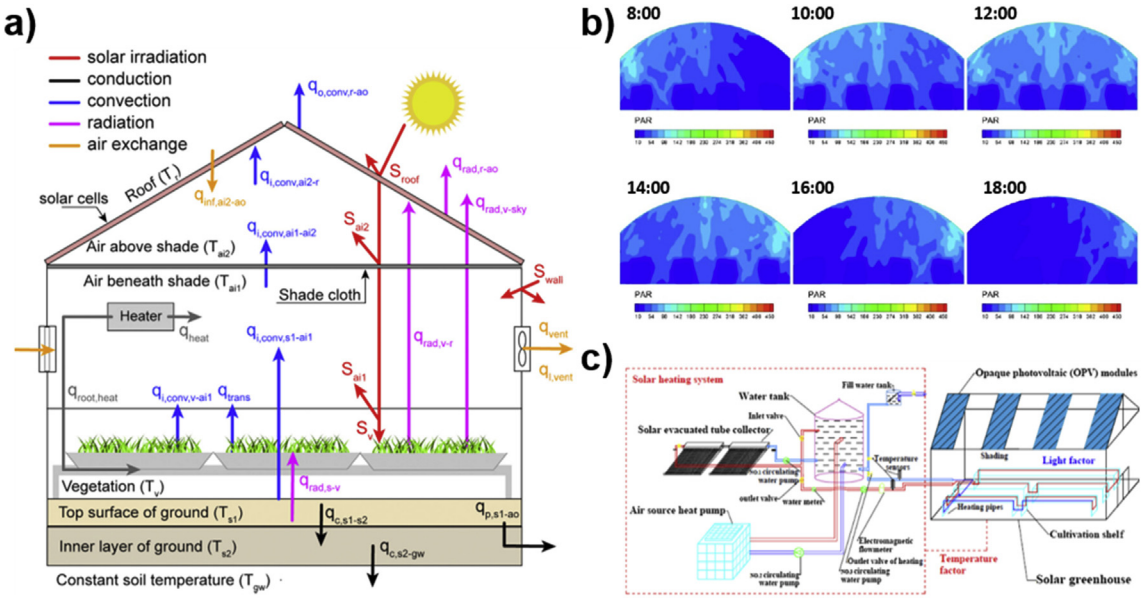

Fig. 2. Simulation of greenhouse integrated with semitransparent OPVs. (a) Schematic of the energy fluxes for greenhouse integrated with semitransparent OPVs. (b) Photosynthetically active radiation (PAR) isocontours. (c) Principal diagram of energy system and layout of the solar greenhouse. (a). Reproduced (a) with permission from ref. [29], (b) with permission from ref. [30], and (c) with permission from ref. [34]. Copyright 2020 Cell Press, 2020 MPDI, and 2020 Elsevier, respectively.

Table 1
Summary of semitransparent OPVs using strategy of active layer material design in Section 4.1.

Active layer	Strategy	V_{OC} [V]	J_{SC} [mA cm^{-2}]	FF [%]	PCE [%]	AVT [%]	CRI/CIE	Ref
PCE10:A078	NIR absorbing donors/acceptors	0.75	20.4 ± 0.8	70 ± 3	10.8 ± 0.5	45.7 ± 2.1	86	[35]
PTB7-Th:IEICO-4Cl	NIR absorbing donors/acceptors	0.725	19.6	59	8.38	25.6	NA	[36]
PTB7-Th:FNIC2	NIR absorbing donors/acceptors	0.727 ± 0.002	21.42 ± 0.48	71.6 ± 1.4	11.1 ± 0.2	13.9	NA	[33]
PBT1-C-2Cl:Y6	Donor-to-acceptor ratio adjustment	0.82 ± 0.01	16.01 ± 0.3	67.2 ± 0.5	9.1	40.1	NA	[38]
D18-Cl:Y6-1O	Donor-to-acceptor ratio adjustment	0.884	19.56	75.31	13.02	20.2	NA	[39]
PDTIDTBT:PCBM	Wide-bandgap donors	0.91	9.8	53.5	4.57	55	NA	[41]
PCE10-2Cl:IT-4F	Wide-bandgap donors	0.817 ± 0.01	14.96 ± 0.20	67.52 ± 0.15	8.25	33	69.2	[42]
PTB7-Th/PBT1-S:$PC_{71}BM$	Ternary/Quaternary systems	0.83	15.6	70.8	9.2	20	NA	[45]
PBDB-TF:Y6/DTNIF	Ternary/Quaternary systems	0.847	22.71	70.16	13.49	22.58	NA	[46]
PBDB-T-2F:Y6/10%DIBC	Ternary/Quaternary systems	0.83	23.43	71.85	13.73	21.6	NA	[47]
PBDB-T/PTB7-Th:ITIC-Th/$PC_{70}BM$	Ternary/Quaternary systems	0.67	9.92	64.82	15.46	63	NA	[48]
PTB7-Th:DTG-IW	Side-chains' direction modification	0.71	14.6	60	6.19	50.4	NA	[49]
PTB7-Th:$PC_{71}BM$: 0.5% DDO	Halogen-free solid additive	0.839	14.44	69.42	8.41	30.8	NA	[50]
PTB7-Th:IEICO-4F/NCBDT-4Cl	Bicontinuous pathways	0.7	21.50	68.5	10.31	20.6	(0.24, 0.28)	[51]
PBDB-T-2F:Y6	Sequential deposition	0.84 ± 0.01	22.51 ± 0.2	68.31 ± 0.3	12.55 ± 0.3	18	92	[52]
J52:IEICO-4F/$PC_{71}BM$	Wide-bandgap donors	0.685	16.9	66.9	7.75	19.9	NA	[4]
PBDB-T-2F:A-2ThCl/A-4Cl/$PC_{71}BM$	Ternary/Quaternary systems	0.86	21.68	70	13.08	23	72.99	[54]

active layers of J52:IEICO-4Cl-, PBDB-T:IEICO-4Cl-, and PTB7-Th:IEICO-4Cl-based devices had PCEs of 6.37%, 6.24%, and 6.97% with AVTs of 35.1%, 35.7%, and 33.5%, respectively. To further enhance the performances of the devices, the thickness of Au of the devices were varied. As a result, a PCE of 8.38% with an AVT of 25.6% was obtained. Similarly, Lu et al. also developed NIR acceptors with high crystallinity: FNIC1 and FNIC2 (Fig. 3b) [33]. Compared with FNIC1, FNIC2 has a better intermolecular stacking capability, which led to a more red-shifted absorption peak and higher crystallinity. The resulted semitransparent device based on PTB7-Th and FNIC2 had a PCE of 11.1% with an AVT of 13.9%, which are promising features for agricultural application with energy generation.

The strategy that uses NIR absorbing molecules in the active layer of semitransparent OPVs effectively enhances the AVT of the devices by reducing the absorption in the visible wavelength range. However, the inevitable drawback is that fewer photon absorption leads to a decreased current density. Namely, there will still be a trade-off between the PCE and the AVT of the semitransparent devices. In addition, although the newly designed donors/acceptors have truly enhanced the AVT of semitransparent devices, these materials suffer from reduced V_{OC} because of the narrower bandgap of them.

4.1.2. Donor-to-acceptor ratio adjustment

Another trade-off strategy is to reduce the amount of visible-light-absorbing donor for higher AVT [37–39]. Sun et al. demonstrated a fibril network strategy that improved the PCE and AVT of semitransparent OPVs simultaneously [38]. A polymer donor PBT1-C-2Cl that can self-assemble into a fibril nanostructure was used as the donor and a NIR-absorbing small molecule Y6 was used as the acceptor. A tiny amount of PBT1-C-2Cl in the blend was proved to form a high-speed pathway for hole transport owing to the finely distributed fibril nanostructure, therefore increasing the AVT. Meanwhile, the acceptor Y6 is still providing sufficient light absorption. Implementing this strategy, the optimized semitransparent OPVs had a high PCE of 9.1% with an AVT of over 40%

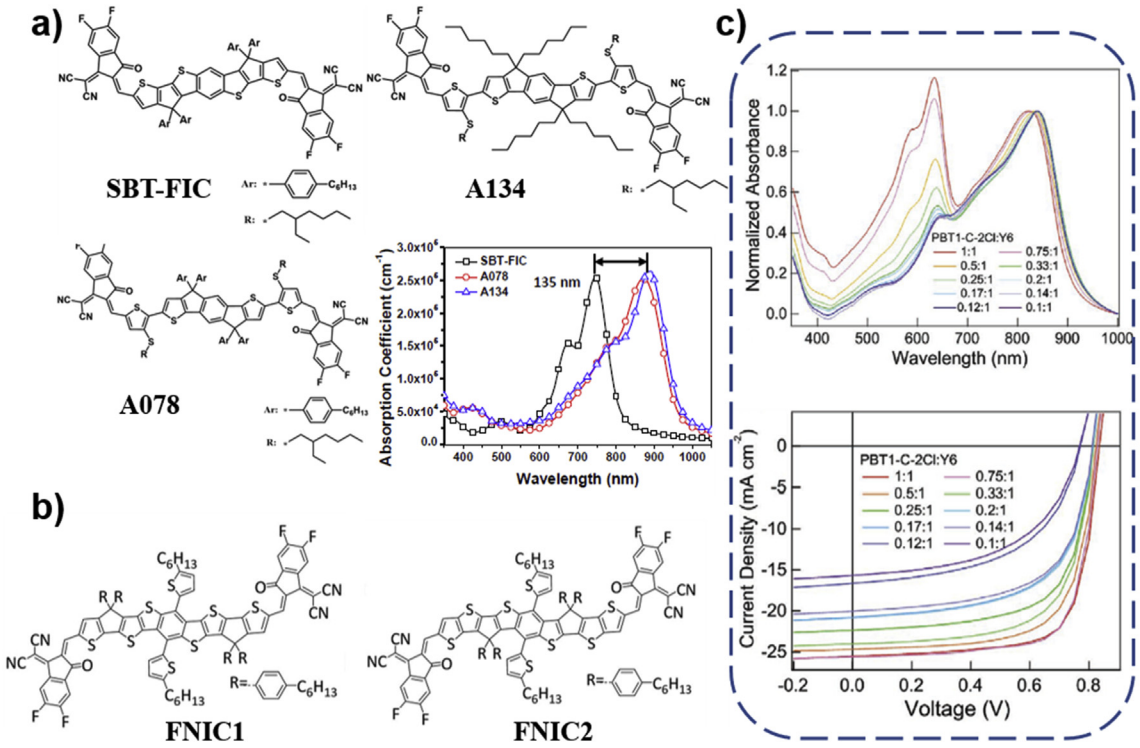

Fig. 3. Strategies of NIR absorbing donors/acceptors and donor-to-acceptor ratio adjustment. (a) Molecular structural formulae and UV−vis absorption spectra of the SBT-FIC, A078, and A134. (b) Chemical structures of the donor PTB7-Th and acceptors FNIC1 and FNIC2 which are isomers with different crystallinities. (c) UV−vis absorption spectra and J−V characteristics of PBT1-C-2Cl:Y6 blend films with various D/A weight ratios. Reproduced (a) with permission from ref. [35], (b) with permission from ref. [33], and (c) with permission from ref. [38]. Copyright 2020 The Royal Society of Chemistry, 2020 National Academy of Sciences, and 2020 Wiley-VCH, respectively.

and a substantial light utilization efficiency of 3.65% at donor to acceptor (D:A) ratio of 0.25:1 (Fig. 3c). Similarly, Zhang et al. enhanced the AVT of the devices by modifying the D:A weight ratio [39]. The AVT of blend films increased from 30.3% to 47.3% with a decrease of D:A weight ratio from 1.1:1.6 to 0.7:1.6. The resulted device reached a PCE of 13.02% and an AVT of 20.2%. Since the donors have absorption peaks in the visible wavelength region, the reduction of the D:A ratio significantly increased the AVT of the devices. However, insufficient donor in the active layer impeded charge carrier dissociation and transportation, leading to a serious compromise in device PCE.

4.1.3. *Wide-bandgap donors for higher V_{OC}*

Most semitransparent organic solar cells show a low V_{OC} because of the inherent narrow bandgap of the active layer materials, which is proven to be a key limitation for the improvement of the device performances. To solve this problem, large bandgap donors were applied for higher V_{OC} in the semitransparent solar cells [40,41]. Kong et al. synthesized a dithiaindacenone-thiophene-benzothiadiazole-thiophene alternating donor copolymer named PDTIDTBT with good ambient stability, large carrier mobility, and high transmittance (Fig. 4a) [41]. Since PDTIDTBT was stable in air and water, they implemented a wet transfer technique that was used for graphene to the fabrication processes of the semitransparent OPVs. The OPVs based on the PDTIDTBT:PCBM blend had PCEs of 6.1% and 4.75% using silver and graphene top electrodes, respectively. The graphene-based device showed a high AVT of 55%, indicating its potential for roof application.

Although wide-band-gap polymer donors were selected to obtain a high V_{OC}, the absorption in the visible light region of such wide-band-gap polymer donors contributes negatively to the transparency of the devices. Therefore, rational design of active materials to improve the V_{OC} and device efficiency without sacrificing transparency is critical. Lie Chen et al. proposed a new design concept to combine donors and acceptors with low energy levels and overlapping NIR absorption for high-performance semitransparent OPVs [42]. They incorporated chlorine, sulfur, and fluorine functional atoms into the polymer PCE10 to downshift the energy levels of the resulting polymer donors, namely PCE10-2Cl, PCE10-SF and PCE10-2F (Fig. 4b and c). Compared to PCE10, these functionalized polymer donors showed lower energy levels, which led to higher V_{OC}. Since PCE10-2Cl has overlapping absorption with the non-fullerene acceptor IT-4F, the corresponding device obtained both remarkably improved V_{OC}, and comparable *Jsc* in the blends with complementary absorption. As a result, the opyque PCE10-2Cl:IT-4F-based devices achieved a champion PCE of 10.72%, which is the highest among the functionalized PCE10-based devices. For the semitransparent OPV device with PCE10-2Cl:IT-4F, a PCE of 8.25% with an AVT of 33% was achieved without any extra treatment. It indicated that a rational combination of donors and acceptors with overlapping NIR absorption is a promising strategy to produce high performance semitransparent OPVs.

4.1.4. *Ternary/Quaternary systems*

Ternary/Quaternary structure with multiple donors or acceptors in one active layer has been demonstrated as an efficient strategy to improve the device performances. The extra component with complementary absorption can broaden the absorption range, manipulate the active layer morphology, adjust the absorption region of the active layers, and promote the charge dissociation and transportation in the devices. Hence, ternary/Quaternary systems are also applied in the semitransparent OPV device [39,43−48].

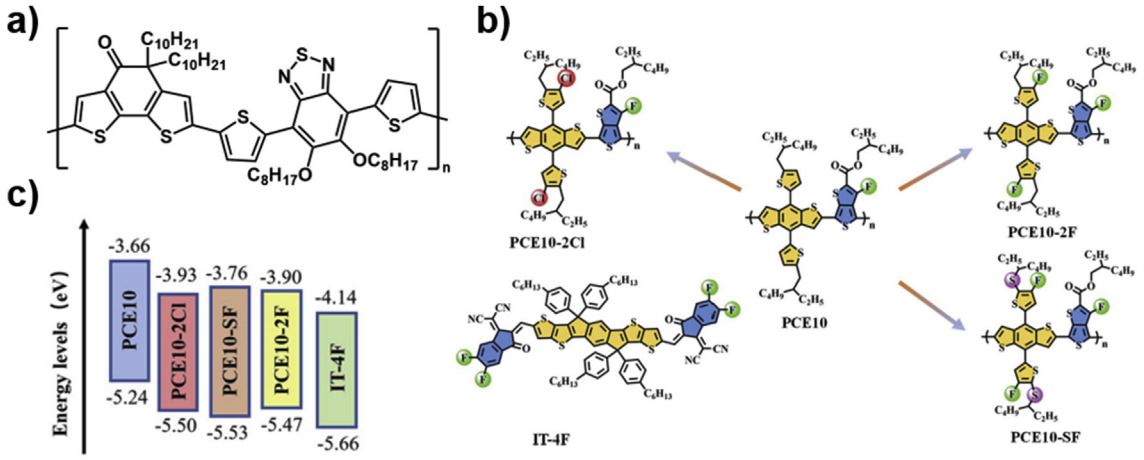

Fig. 4. Strategy of wide-bandgap donors for higher V_{OC}. (a) Schematic of the PDTIDTBT WD–WA copolymer structure. (b) The chemical structures of the polymer donor and NFAs (PCE10, PCE10-2Cl, PCE10-SF, PCE10-2F and IT-4F). (c) Energy levels of PCE10, PCE10-2Cl, PCE10-SF, PCE10-2F and IT-4F. Reproduced (a) with permission from ref. [41], (b, c) with permission from ref. [42]. Copyright 2019 National Academy of Sciences, 2021 The Royal Society of Chemistry, respectively.

Sun et al. developed a ternary structure with broader light absorption and smoother morphology [45]. Semitransparent ternary solar cells were fabricated using a wide-bandgap (E_g = 2.10 eV) polymer donor, PBT1-S, as the third component (Fig. 5a). They found that the addition of a small amount of PBT1-S to PTB7-Th:$PC_{71}BM$ blend had a negligible influence on the AVT and the color perception of the device. The addition of PBT1-S extends the active layer absorption spectra from 400 to 800 nm. A PCE of 9.2% was achieved by the champion ternary device with a AVT of 20%. Zheng et al. synthesized a ladder-type dithienonaphthalene-based acceptor (DTNIF) with a high-lying lowest unoccupied molecular orbit (LUMO) energy level as the third component material for their ternary OPVs (Fig. 5b) [46]. Due to the higher LUMO level of DTNIF, the V_{OC} of the ternary devices based on PBDB-TF:Y6:DTNIF were larger than the V_{OC} of the binary devices based on PBDB-TF:Y6. Morphological investigations indicated that the incorporation of DTNIF could also lead to enhanced crystallinity and closer the π–π stacking of the active layer, resulting in more balanced and effective charge transport. The resulted device shows increased PCEs with higher values in V_{OC}, J_{SC}, and *FF*. Consequently, an exceptional PCE of

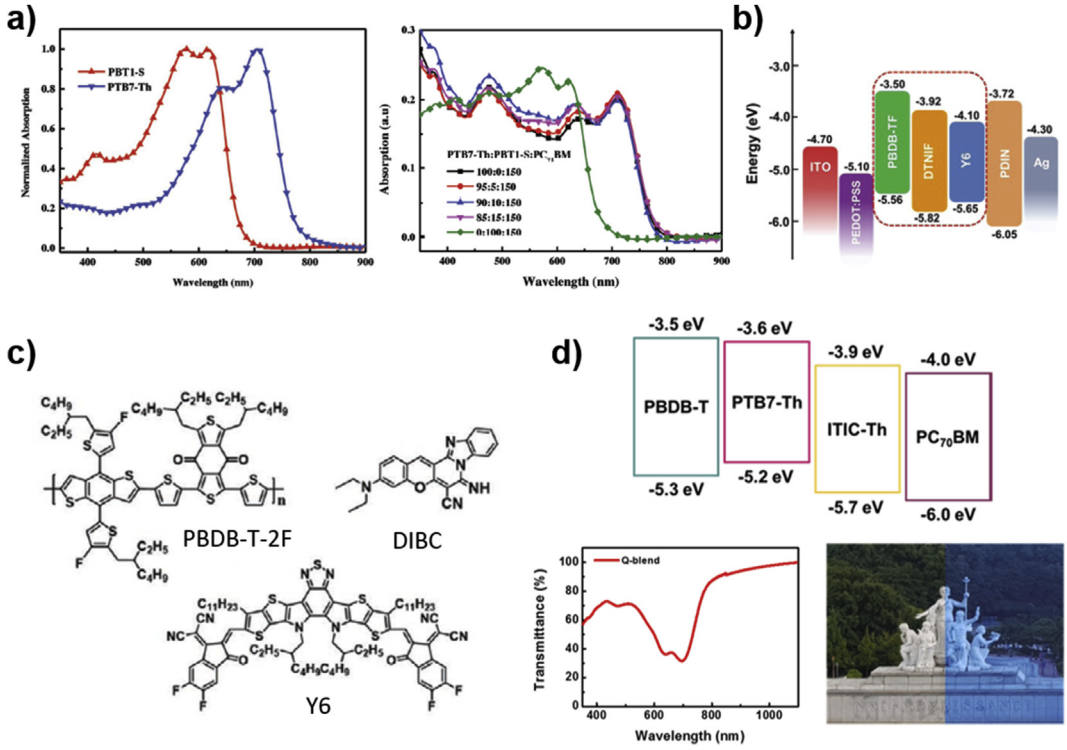

Fig. 5. Strategy of ternary/quaternary systems. (a) UV–vis absorption spectra of neat PBT1-S and PTB7-Th films, the binary and ternary films with different PBT1-S contents. (b) Energy level diagram of PBDB-TF, DTNIF, and Y6 as well as the electrodes and interface layers. (c) Molecule structures of PBDB-T-2F, Y6, and DIBC. (d) Energy levels and transmittance spectrum of the Q-blend film, and a photograph taken without (left) and with (right) filtering by the semitransparent device. Reproduced (a) with permission from ref. [45], (b) with permission from ref. [46], (c) with permission from ref. [47], and (d) with permission from ref. [48]. Copyright 2018 Wiley-VCH, 2020 The Royal Society of Chemistry, 2021 Wiley-VCH, and 2019 Elsevier, respectively.

13.49% was achieved for the corresponding semitransparent ternary OPV with an AVT of 22.58%.

Tao et al. fabricated a ternary semitransparent OPV with a high PCE of 14% and a high AVT of 21.60% by adding an organic small molecule material DIBC into the PBDB-T-2F/Y6 active layer (Fig. 5c) [47]. DIBC interacted with Y6 via an intramolecular hydrogen bond, resulting in higher PCE of the PBDB-T-2F:Y6:10% DIBC-based ternary devices than the binary devices. Besides, as the active layer thickness increased from 70 to 150 nm, all opaque devices achieved high PCEs over 16%. It proved that the hydrogen bonds can enhance the film thickness tolerance of the device. By introducing a proper amount of hydrogen bond, the bimolecular recombination and trap-assisted recombination can be successfully inhibited, leading to an improved *FF* of the device. Moreover, a proper amount of hydrogen bond can enhance the crystallization of the acceptor, promote the transport of electrons, and balance the transport of charges. Besides, the ternary devices based on hydrogen bond demonstrated superior light and thermal stabilities than the binary devices. These results indicated that the hydrogen bond strategy was an effective method to achieve semitransparent OPVs with high performance and high transmittance.

For quaternary systems, Ko et al. developed highly efficient semitransparent OPVs involving non-fullerene small molecules (Fig. 5d) [48]. Their semitransparent quaternary OPVs showed a broadened absorption range and exhibited a PCE exceeding 15% (~15.46%) under indoor lighting. They believed that the quaternary-blend system could operate efficiently under any irradiation conditions (both indoor and outdoor lighting) and via tuning the quaternary components, they would be able to further expand its applicability to different practical applications.

4.1.5. Other strategies

Several other novel strategies have also been developed for the semitransparent devices. Yang et al. improved the morphology of the active layer's transparency by modifying the direction of the side-chains [49]. They synthesized two isomeric NFAs based on DTG (DTG-IW with inward-facing side chains and DTG-OW with outward-facing side chains). The inward-facing side chains on the backbone resulted in extremely confined face-on crystallites in the solid state (Fig. 6a). It led to a semitransparent OPV device with a PCE of 6.19% and a transmittance of 50.4% in the green wavelength region.

Moreover, Tao et al. developed a halogen-free solid additive, 1,10-decanediol (DDO) to enhance the PCEs of the semitransparent OPVs (Fig. 6b) [50]. The addition of DDO has led to improved the crystallinity of the polymer, better miscibility between donor and acceptor, and controlled vertical distribution of molecules. Furthermore, the addition of DDO ensures good film thickness tolerance of the semi-transparent OPV. The device achieved a high PCE of 9.71% with a high AVT of 30.8%.

Han et al. developed bicontinuous pathways and incorporated them in semitransparent polymer solar cells with enhanced charge transportation and higher J_{SC} [51]. They selected PTB7-Th as the donor and IEICO-4F as the acceptor. The problem to solve is that IEICO-4F tends to form strong aggregation due to its planar conformation. To suppress the intense aggregation, an amorphous molecule NCBDT-4Cl miscible with IEICO-4F was added. It raised the nucleation barrier of IEICO-4F as it can be dispersed evenly in the IEICO-4F phase (Fig. 6c). They reported a reduction in the growth time of IEICO-4F was reduced from 122 s to 45 s by incorporating 20 wt% NCBDT-4Cl, resulting in reduced aggregation of IEICO-4F. Inside the PTB7-Th matrix, the well-dispersed small IEICO-4F aggregates could form refined bicontinuous pathways. The optimized device achieved a PCE of 10.31% with an AVT of 20.6%.

Besides, Wei et al. developed a sequential deposition (SD) strategy, which involves the individual deposition of a polymer donor layer and a small-molecule acceptor layer as the active layer. The diffusion of molecules occurred at the interfacial region, and formed a pseudo p−i−n structure (Fig. 6d) [52]. PBDB-T-2F/Y6 semitransparent OPVs were fabricated with two active layer thicknesses, 115 nm and 85 nm. At 115 nm, the SD (D:A/75:40 nm) and BHJ devices (D:A/1:1.2 w) provided the champion PCEs of 12.91% (AVT of 14.5%) and 12.77% (AVT of 13.4%), respectively. At 85 nm, the SD (D:A/45:40 nm) and BHJ devices (D:A/1:1.2 w) provided PCEs of 12.22% (AVT of 22.2%) and 11.23% (AVT of 16.6%), respectively. The comparison between different PCE and AVT values indicated that SD devices had better performances than the BHJ devices at a given active layer thickness, and the SD structures demonstrated more pronounced enhancements of PCEs and AVTs than the BHJ structures when the active layer thickness is reduced.

4.1.6. Special designs for semitransparent OPVs for agricultural application

Too meet the requirements of the agricultural application, unique active layer materials are brought to discussion. Different from semitransparent OPVs that simply require high transparency at the visible wavelength range, the OPVs for agricultural applications like greenhouse roofs need to circumvent the absorbance range of the plant photosynthesis. Fig. 7a shows the absorbance ranges of the different plant photosensitive pigments [53]. Among them, chlorophyll A and B are the most common ones for the agricultural plants. Noticing that these two pigments have absorption range from around 360 nm to 500 nm, we should aim to achieve high transparency at this blue/violet range instead of the whole visible wavelength range when choosing the donors/acceptors for the active layers.

With this consideration, Yip et al. developed a semitransparent OPV with a selectived wavelength range corresponding to the proper transmission spectrum for plant growth [4]. By combining a wide bandgap polymer donor (J52) with a near-infrared absorbing NFA (IEICO-4F) and a high electron mobility fullerene acceptor ($PC_{71}BM$), their semitransparent OPV achieved a PCE of 7.75%. The addition of $PC_{71}BM$ into J52:IEICO-4F binary blend contributed to the suppressed trap-assisted recombination, enhanced the charge extraction, and improved the V_{OC} simultaneously. And a defined crop growth factor of 24.8% was achieved. The absorption spectra of chlorophylls, the photoreceptors in green plants, matched perfectly with the transmittance spectra of the semitransparent OPV devices. Therefore, semitransparent OPV, by providing adequate illumination conditions for photosynthesis and plant growth, becomes a competitive candidate for photovoltaic greenhouse applications (Fig. 7b).

Similarly, Li et al. developed a spectrally engineered semitransparent OPVs using quaternary blends of PBDB-T-2F, A-2ThCl, A-4Cl, and $PC_{71}BM$ (Fig. 7c) [54]. They observed that the quaternary blends created suitable photon transmission windows suitable for plant absorption and conferred excellent photovoltaic properties with non-halogenated solvent fabrication. PCEs of 13.08% were achieved by the resulted semitransparent OPVs. The plants grew favorably with a plant growth factor of 24.7% under the semitransparent OPV filtered lights, which was comparable with that under transparent glass (Fig. 7d).

4.2. Electrode developments

Compared with inorganic photovoltaics, OPVs possess semitransparent features which provide opportunities for power-generation windows or greenhouse applications. Most studies are focused on the material side to improve the transparency of the

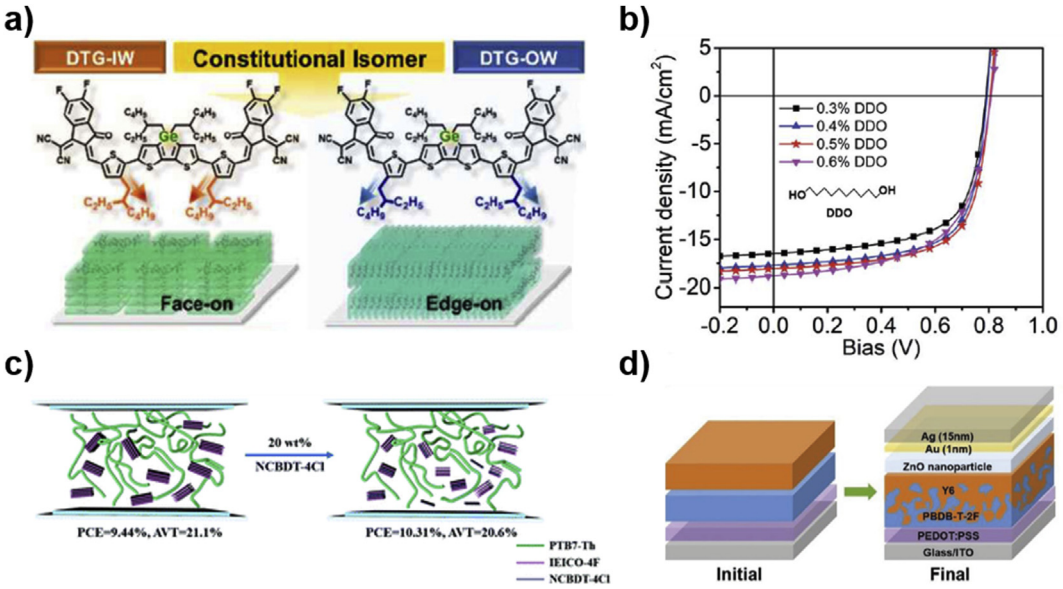

Fig. 6. Other strategies of the active layer material design. (a) Configurations of DTG-IW and DTG-OW. (b) *J*–*V* curves of DDO-containing devices with different doping ratios. (c) Schematic of the PTB7-Th/IEICO-4F active layers with and without NCBDT-4Cl. (d) Schematic representation of the two-step SD processing and the final device structure. Reproduced (a) with permission from ref. [49], (b) with permission from ref. [50], (c) with permission from ref. [51], and (d) with permission from ref. [52]. Copyright 2020 Wiley-VCH, 2019 The Royal Society of Chemistry, 2021 The Royal Society of Chemistry, and 2021 Wiley-VCH, respectively.

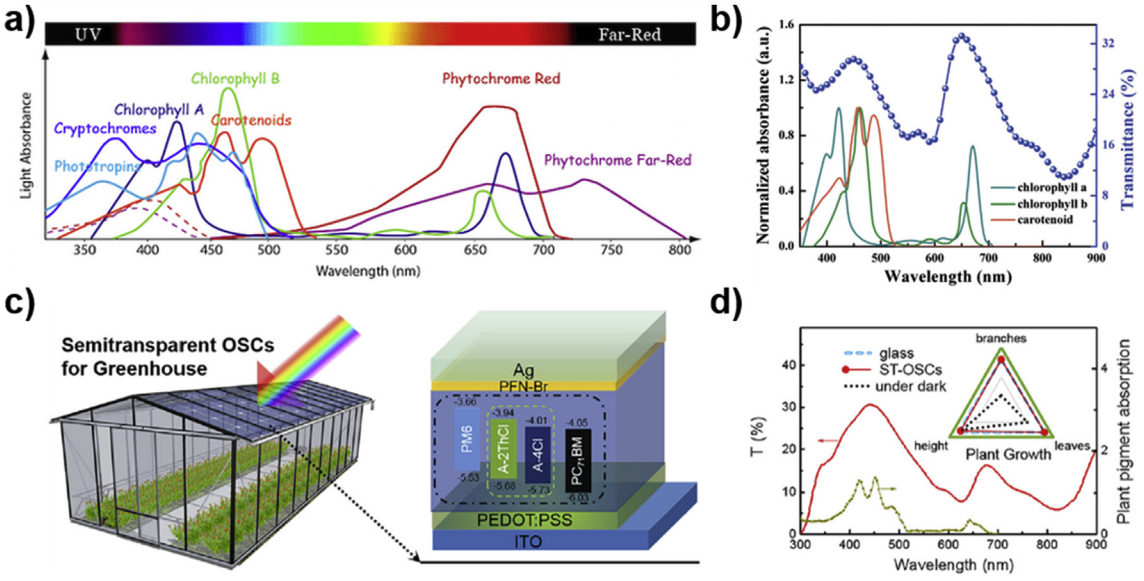

Fig. 7. Special designs for semitransparent OPVs for agricultural application. (a) Absorption wavelengths of plant photosensitive pigments. (b) Transmittance spectra of the J52:IEICO-4F:$PC_{71}BM$ (1:0.9:0.6) device with 15 nm Ag film as transparent cathode and optical absorption spectra of chlorophyll *a*, chlorophyll *b*, and carotenoid. (c) Greenhouse, device structure, and energy diagrams of PBDB-T-2F, A-2ThCl, A-4Cl, and $PC_{71}BM$. (d) Transmittance spectra of semitransparent devices and plant growth evaluation including height, branches, and leaves after 90 h of continuous illumination through different roofing materials. Reproduced (a) with permission from ref. [53], (b) with permission from ref. [4], and (c, d) with permission from ref. [54]. Copyright 2021 LED Grow Lights HQ, 2019 Wiley-VCH, and 2021 Cell Press, respectively.

device. However, the design of the electrodes is also crucial for semitransparent OPVs to reach high performance.

The most common electrodes of OPVs are mainly based on metals due to their low sheet resistances (high conductivity). However, the common metal electrodes are mostly opaque, leading to low transmittance. For semitransparent OPVs, it is important for the electrodes to fulfill high-transparency and high conductivity at the same time. In the following passage, various methods strived to maintain a decent conductivity and high transparency of electrodes of semitransparent OPVs will be discussed. We divide the topics into color electrodes, conducting polymer electrodes, ultrathin metal electrodes, sliver-nanowire based electrodes, and the influences of electrodes on agricultural applications. The corresponding strategies and the related device performances are summarized in Table 2.

4.2.1. Color filter (CF) electrodes

In pursuit of the color change of semitransparent OPVs, most of the studies focus on the active layer. The implementation of a color-filter (CF) electrode could be another approach to display various

Table 2
Summary of semitransparent OPVs using strategy of electrode developments in Section 4.2.

Active layer	Electrode	PCE [%]	AVT [%]	CRI/CIE	Ref
PTB7-Th:$PC_{71}BM$	ITO/blue, green and red Ag—TiO_x—Ag color filter (CF)	4.54 (w/Blue filter)	NA	NA	[55]
PTB7-Th:ITIC	ITO and Ag—TiO_2—AcAc—Ag (orange)	5.24 ± 0.75	NA	NA	[56]
PBDB-T-2F:N3/Y6	Al:Ag/dielectric stacks (LiF and NPB)/Al:Ag/dielectric stacks (LiF and NPB)/carbon fluoride spectrally selective electrode (SSE)	15.07	NA	(0.16, 0.02)	[57]
P3HT:PCBM	PEDOT:PSS 500 and PEDOT:PSS 500	0.47	NA	NA	[58]
PBDB-T-2F:Y6	Al/Ag and D-PEDOT:PSS/PET	12.59	17	(0.2287, 0.2213)	[60]
C60:F4-ZnPc	ITO and 1 nm Au and 7 nm Ag	4.6	NA	NA	[62]
PTB7:$PC_{71}BM$	TiO_2-3-4 nm Ag-ITO and Ag	8.34	NA	NA	[63]
PTB7-Th:BT-CIC/TT-FIC	ITO w/ARC and 16 nm Cu—Ag w/OC	8.0 ± 0.2	44.2 ± 1.4	(0.280, 0.335)	[64]
PBDTT-DPP:PCBM	ITO and TiO_2/AgNW-based composite electrode	4.02	NA	NA	[69]
PV2000:$PC_{70}BM$	Inkjet-printed AgNWs	4.3	NA	NA	[70]

colors with focused spectrum. Hyun et al. reported a colorful and semitransparent OPVs using the Ag—TiO_x—Ag CFs based with the active layer materials of PTB7-Th:$PC_{71}BM$ [55]. The color of the light passed through the CF-electrode was changed by the cavity resonance of the Ag—TiO_x—Ag architecture with high spectral purity, and the positions of the transmission peaks were determined by the thickness of TiOx. When compared with normal semitransparent OPV (ITO/ZnO/PTB7-Th:$PC_{71}BM$/MoO_3/Ag/MoO_3), the red, blue, and green CF-integrated OPVs showed an enhancement of J_{SC} over 30% due to the contribution of the reflected light with complementary spectrum of the color CF-integrated OPVs appearance. Note that the semitransparent OPVs devices with CF electrodes showed no compromised performance but have additional color appearance for window applications. Besides, Kim et al. demonstrated a solution-processed TiO_2-AcAc as the dielectric component for preparing the color filter-integrated OPVs [56]. Compared with e-beam-processed TiO_2 based CF, the non-invasive solution processed CF based OPVs presented superior V_{OC} and *FF* which lead to a higher PCE. Recently, Tang et al. reported a spectrally selective electrodes (SSEs) for semitransparent OPVs inspired by the beetle cuticle (Fig. 8a) [57]. The beetle cuticle inspired SSE was combined with the induced transmitting filter, conductive metal, antireflective coating, and hydrophobic surface. The architecture of the SSE was Al:Ag/dielectric stacks (lithium fluoride and N,N′-bis(naphthalen-1-yl)-N,N′-bis(phenyl)benzidine)/Al:Ag/dielectric stacks (lithium fluoride and N,N′-bis(naphthalen-1-yl)-N,N′-bis(phenyl)benzidine)/carbon fluoride. Compared with the device with only Al:Ag electrode, the SSE based device showed an improvement of PCE from 13.7% to 15.1% due to the contribution of SSE's reflection. In addition, a maximum peak transmittance approaching 30% and a high color purity approaching 100% were observed.

4.2.2. Conducting polymer electrodes

For conducting polymer electrodes, Jen et al. replaced both the anode and cathode with PEDOT:PSS in inverted solar cells [58]. The flexible nature of the conjugated polymer of PEDOT:PSS showed better mechanical stability than ITO-based electrode. The PEDOT:PSS as the cathode-based device showed high retention PCE of 92% compared with ITO-based (ca. 50%) after 300 bending cycles. With ITO as the cathode and PEDOT:PSS as the anode, the device showed a PCE of 2.51%, whereas the device based on P3HT:PCBM with both PEDOT:PSS anode and cathode showed a low PCE of 0.47%. Later, Zhan et al. introduced PH1000 as the bottom and top electrode with P3HT:IDT-2BR as the active layer [59]. The flexible device exhibited a PCE of 2.9% with an AVT of ca 50%. In addition, devices with the same structure and contain fullerene-based active layer (P3HT:$PC_{61}BM$) were fabricated. The PCE of non-fullerene-based devices decreases by 12% from the original PCE with 250 bending cycles and the PCE of fullerene-based devices decreased by a larger amount of 23% with the same bending cycles. In recent, Ge et al. reported a foldable-flexible OPV (FS-OPV) with D-PEDOT:PSS/PET as the electrode and substrate to replace ITO/glass, processed with the polyhydroxy compound (xylitol) microdoping and acid treatment (Fig. 8b) [60]. The hydroxylated surface of xylitol component inside the doped D-PEDOT:PSS formed a hydrogen bond with the carbonyl group on the PET substrate. The enhancement of the intermolecular force improved the mechanical properties. The xylitol doping FS-OPV based on PBDB-T-2F:Y6 yielded a PCE of 14.2%, maintaining larger than 80% of the original PCE after 1,000 folding cycles. The semitransparent OPV based on the same active layer yielded over 10% PCE with an AVT over 20%.

4.2.3. Ultrathin metal electrodes

In general, the opaque OPVs use highly conductive metals as the electrode (such as Ag, aluminum (Al), gold (Au), etc.) with an around 100 nm thickness. The thick electrode brings low light transmittance of the device. In order to fabricate a semitransparent OPV, researchers first used a thinner electrode that compromised the conductivity for high transparency [61]. However, a single thin metal layer possesses relatively high resistivity due to surface roughness and grain boundaries.

Leo et al. introduced an additional high surface energy seed layer (calcium (Ca), aluminum(Al), and Au) on the bottom of Ag in the dielectric/metal/dielectric (DMD) structure [62]. The only 1-nm-thick seed layer improved the wetting of Ag on the substrate, helping to form a continuous and smooth layer. As a result, the electrode with the seed layer showed a lower sheet resistance of 19 Ω/sq than the pure Ag electrode and ITO (32 Ω/sq) electrode. The PCE of the device based on C60:F4-ZnPc reached 4.7%, which was close to the PCE of the bottom-illuminated OPV devices with ITO electrode. The optimized devices with 1 nm of gold and 7 nm Ag as the electrode showed a high transmittance of 83% at the wavelength of 580 nm, which is better than that of the ITO-based OPV devices. Similar work was demonstrated by Pruneri et al. [63]. They reported a transparent electrode with a structure of TiO_2—Ag—ITO in the inverted OPV structure. With the aid of the TiO_2, ultrathin Ag layer (3—4 nm) forms a continuous and smooth layer due to the better wetting property. The average optical transmittance of the TiO_2—Ag—ITO based electrode achieved a high value of 87.6% in the range of 375 nm—700 nm. This electrode structure not only provided a good transparency, but also exhibited relatively low sheet resistance with a value of 6.2 Ω/sq, which was lower than that of the traditional ITO based electrode. In addition, the TiO_2—Ag—ITO based electrode remained almost 95% in low resistance after 1,000 bending cycle. The device with TiO_2—Ag—ITO based electrode and PTB7:$PC_{71}BM$ active layer achieved a PCE of 8% with decent mechanical properties. Forrest et al. demonstrated a semitransparent OPV consisted of NIR absorbers (PTB7-Th: BT-CIC: TT-FIC) with thin Cu—Ag alloy electrode (Fig. 8c) [64]. The Cu—Ag electrode provided a much better average transmittance (72%) from 400 nm to 650 nm

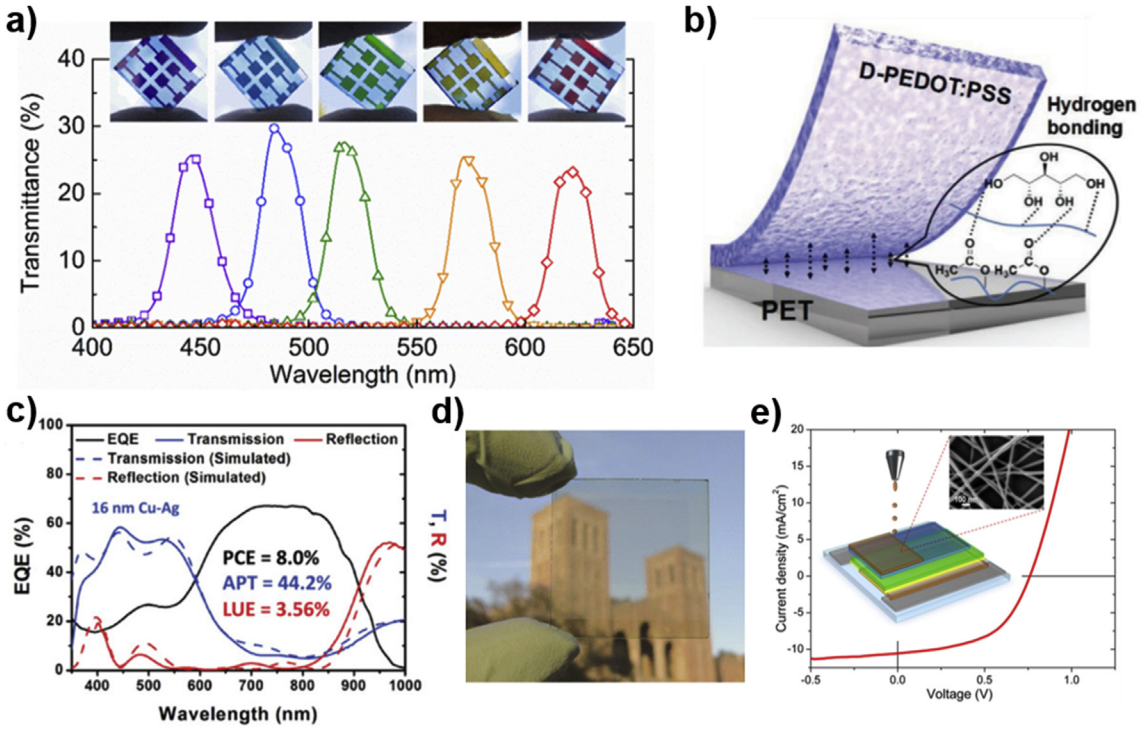

Fig. 8. Electrode developments of semitransparent OPVs for agricultural application. (a) Digital photographs of semitransparent OPVs with various SSEs. (b) The schematic diagram of hydrogen bond and van der Waals bond effect on the D-PEDOT:PSS/PET interface. (c) Measured and simulated optical transmission, reflection, and external quantum efficiencies of the semitransparent cells with 16 nm Cu–Ag. (d) Photograph of a visibly transparent polymer solar cell. (e) Inkjet-printed silver nanowire percolation networks as electrodes and the device performance. Reproduced (a) with permission from ref. [57], (b) with permission from ref. [60], (c) with permission from ref. [64], (d) with permission from ref. [69], and (e) with permission from ref. [70]. Copyright 2020 American Chemical Society, 2020 Wiley-VCH, 2019 American Chemical Society, 2012 American Chemical Society, and 2016 Elsevier, respectively.

than the ones provided by Ag (average transmittance of 58%) or Au–Ag (average transmittance of 64%) electrodes. With the addition of the outcoupling layer and the antireflection coating, the visible transmittance of the device increased and the reflection in the near infrared region of the device also increases. The optimized OPV achieved a PCE of 8% with a high average photopic transmittance of 44.2% and LUE of 3.6%. Besides, the neutral semitransparent OPVs were also fabricated. The device showed a PCE of 5.8% with an average photopic transmittance of 44.3% and a CRI of 87.

4.2.4. Silver nanowire based electrodes

The low temperature and solution processes of silver nanowire (AgNWs) provide another good choice for the electrode to fabricate high performance semitransparent OPVs. The AgNWs electrodes can be prepared with many approaches such as drop casting, lamination, spray coating and inkjet printing [65–68]. With the high transmittance (up to 90%) and low sheet resistance (lower than 15 Ω/sq), the semitransparent OPV devices based on the AgNWs show good performance. Yang et al. demonstrated a visibly transparent OPV with a device structure of ITO/PEDOT:PSS/PBDTT-DPP:PCBM/TiO_2/AgNW-based composite electrode (Fig. 8d) [69]. They used the near-infrared polymer PBDTT-DPP in the active layer with AgNWs as the top transparent electrode. The PCE of the device achieved up to 4% with an average light transmittance of 61% within the visible range (400 nm–650 nm). A high visible transparency of 66% at 550 nm was achieved in the same device. The device showed similar performance under the same incident light beam but from different side of the semitransparent OPV device. Similarly, Brabec et al. demonstrated a non-ITO based semitransparent OPV with the structure of glass/AgNWs:ZnO/PV2000:PCBM/PEDOT:PSS/AgNWs (Fig. 8e) [70]. The AgNWs was prepared by inkjet printing. The printed AgNWs electrodes performed well with a PCE of 4.3% in the 1 cm^2 area device. Overall, the conductivity and transmittance of inkjet printing AgNWs were close to those of AgNWs prepared by slot die and spray coating.

4.2.5. Electrodes influences for agricultural application

The different electrodes of the semitransparent OPV may affect the plant growth for greenhouse application. Ge et al. fabricated the modified D-PEDOT:PSS-based semitransparent OPV with the active layer of PBDB-T-2F:Y6 [60]. The low reflectivity in the range of 400–550 nm of the designed semitransparent OPV facilitates photosynthesis process for plants. It showed that more visible light, which was responsible for the plant's growth within greenhouses, can transmit through the device. The CRI coordinate varied with the thickness of the Ag electrode: i.e., the device with 10 nm Ag presented a coordinate of (0.2431, 0.2462), and the device with 20 nm Ag presented a coordinate of (0.2307, 0.2232). The thicker of the Ag electrode resulted in more blue-shifted of the color appearance. In addition, they also demonstrated the plants growth in three different situations, including under direct sunlight, under direct sunlight with the semitransparent OPV, and in the dark. The plant growth under sunlight and with the semitransparent OPV were similar, which are relatively sturdier than the one in the dark.

4.3. Structural modification

To further promote the transmittance and photoelectric performances of the organic solar cells, special modifications of the device structures were applied. These structural modifications can be mainly divided into two categories: (1) extra interlayer, and (2) photonic reflector. Both modifications have been widely reported to

effectively adjust the optical distribution across the OPV devices or selectively reflect NIR light back to the interior, thus increasing the photon utilization in the NIR range. The additional function of the interlayers inside the device structure is to improve the interface contact and carrier transportation. However, as an additional layer inside of the semitransparent devices, it might also provide extra internal resistance that impair the photoelectric performances of the devices. The strategies of structural modification and corresponding device performances are summarized in Table 3.

4.3.1. Interlayer modification

Because of the contradiction of the PCE and AVT of the semitransparent OPVs, it is difficult to maintain the considerable transmittance and improve the device performances at the same time within the conventional device architecture. Hence, the interlayer is regarded as an alternative solution. The insertion of an extra buffer layer has been proven to enhance the charge transportation at the interfaces and modify the optical distribution across the device.

Tan et al. developed a novel cathode buffer layer aluminum(III) acetylacetonate ($Al(acac)_3$) with suitable energy levels through mild spin-coating with a heat treatment process at low temperature (Fig. 9a) [71]. A 10 nm $Al(acac)_3$ thin film conferred high transmittance up to 95%, in the visible and NIR regions. It also had suitable energy levels that ensured a smooth electron transport and collection. The introduction of the $Al(acac)_3$ layer into the semitransparent OPVs enabled the PBDB-T-2F:Y6 based devices to achieve an efficiency of 12.41% with an AVT of 25.33% in the wavelength range of 370 nm to 740 nm. Also, the semitransparent OPVs with encapsulation retained 60% of the initial PCE over 60 hours of continuous illumination. The results indicated that $Al(acac)_3$ was a promising cathode buffer layer for semi-transparent organic solar cells.

Hoex et al. used the atomic layer deposition (ALD) to make ultrathin TiO_x as the interface layer between the ZnO electron transport layer and the active layer (Fig. 9b) [72]. Only two TiO_x ALD cycles was proven to effectively passivate the interface and reduce the series resistance. As a result, the charge transport process between the electron transport layer and the active layer was facilitated. Semitransparent OPVs fabricated with interface modification strategy reached an average PCE of 10.46% with an AVT of 19.61%. As for the interface between the electron transport layer and the active layer, Tan et al. chemically precipitated SnO_2 colloidal particles as an electron collection interlayer (Fig. 9c) [73]. Owing to its high transparency and reflective index, the SnO_2 layer can effectively tune the light-distribution of the incident light within the whole multilayered semitransparent OPVs. The deep blue device showed the highest PCE of 12.88% with AVT of 25.60% in the wavelength range of 370 nm to 740 nm. As implied by the above results, the interfacial engineering is an effective approach to achieve high performance OPVs with vivid colors, high transparency, and enhanced efficiency. Similarly, Yip et al. introduced a versatile interlayer, PF3N-2TNDI, for high performance semitransparent OPVs (Fig. 9d) [74]. They claimed that the interlayer acted as an efficient electron transport layer to improve electron extraction of the cathode. Simultaneously, the interlayer could act as an optical spacer to modulate and maximize the optical field and charge generation rate distribution. Besides, the PF3N-2TNDI interlayer, once in contact with the donor in the BHJ film, produced additional photocurrent and promoted the growth quality of the ultrathin Ag film as efficient transparent electrode for the semitransparent OPVs. When further combined with optical model, devices with PCEs over 6% and AVTs of over 30% were achieved.

At the interlayer between the hole transport layer and the active layer of OPVs, Shen et al. used the Au/Ag alloy nanoparticles (NPs) to decrease the resistance and enhance the efficiency via the localized surface plasmon resonances (LSPR) effect (Fig. 9e) [75]. The PCE improved dramatically from 5.50 ± 0.15% to 7.15 ± 0.17% with 17 ± 1.2 nm Ag and 8 ± 0.5 nm Au NPs. The interlayers in semitransparent solar cells enhanced the charge extraction and transportation at the interfaces, and provided high transmittance and electron mobility. The interlayers in the semitransparent solar cells are crucial to enhance the charge transportation and extraction at the interfaces. Potentially, it may also play an important role in the agricultural applications of the organic solar cells. Acting as an extra protective layer of the organic active layer, some of the interlayers with hydrophobicity may also enhance the environmental stability of the solar cells.

4.3.2. Photonic reflector

Besides the extra interlayer inside of the solar cell architecture, external photonic reflector at the top or the bottom of the semitransparent devices are also demonstrated as a powerful strategy to promote the performances of the solar cells. The photonic reflectors can selectively reflect the NIR light back to the devices. For example, Chen et al. used a TeO_2 capping layer on top of the ultra-thin Ag to improve the light-absorbing selectivity [76]. The light utilization efficiency was significantly improved to 3.95 ± 0.02% with the highest efficiency of approximately 4.06%. More usually, instead of monolayer of metal oxide, a photonic reflector is consisted of an alternative stacking of transparent dielectric layers with a large contrast of refractive indexes to modulate the reflectance and transmission of the incident light.

Yip et al. simulated tens of millions of device configurations for photo crystal enhanced semitransparent OPVs to investigate their optical properties [77]. They found that the single-pair photo

Table 3
Summary of semitransparent OPVs using strategy of structural modification in Section 4.3.

Active layer	Interlayer/Photonic reflector	PCE [%]	AVT [%]	CRI/CIE	Ref
PBDB-T-2F:Y6	$Al(acac)_3$ interlayer	12.41	25.33	(0.2569, 0.2571)	[71]
PBDB-T-2F:N3	ultrathin TiO_x interlayer	10.46	19.61	Close to 100	[72]
PBDB-T-2F:Y6	SnO_2 colloidal particles interlayer	12.88	25.60	97.6	[73]
PTB7-Th:$PC_{71}BM$	PF3N-2TNDI interlayer	6	30	96.6	[74]
PTB7-Th:$PC_{71}BM$	Au/Ag alloy nanoparticles (NPs) interlayer	7.15 ± 0.17	Over 20	95	[75]
PTB7-Th:H3	TeO_2 capping layer	8.26 ± 0.12	50.09	71.29	[76]
PTB7-Th:IEICO-4F	Single-pair photo crystals: LiF/MgO_3	11	30	NA	[77]
PTB7-Th:BT-CIC/TT-FIC	Outcoupling (OC) layer: CBP/MgF_2/CBP/MgF_2 and distributed Bragg reflector (DBR): 12.5 pairs of SiN_x and SiO_2	8.0 ± 0.2	44.2 ± 1.4	(0.280, 0.335)	[64]
PTB7-Th:$PC_{71}BM$	one-dimensional photonic crystal (1DPC): TiO_2/SiO_2	5.20	24	(0.35, 0.36)	[78]
J71:ITIC	polymer flexible one-dimensional photonic crystals (F-1DPCs)	7.58	13.3	(0.25, 0.1)	[79]
PTB7-Th:$PC_{71}BM$	extra added layer (EAL)/1DPCs: WO_3/LiF	9.36 ± 0.16	14.31 ± 0.65	(0.317, 0.320)	[80]
PTB7-Th:$PC_{71}BM$	Antireflective (AR) layer: subwavelength architectured polydimethylsiloxane (SWA-PDMS)	8.52	26.2	90	[81]

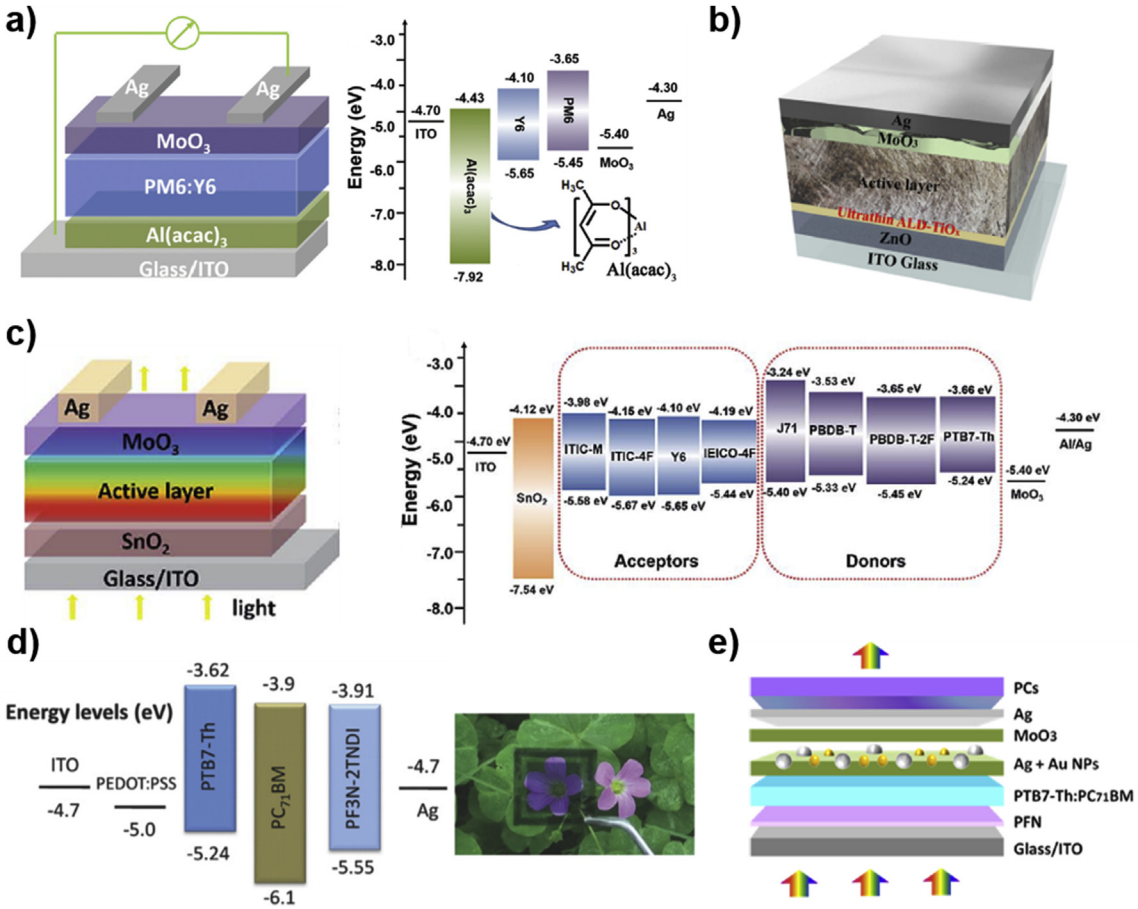

Fig. 9. Interlayer modifications of semitransparent OPVs for agricultural application. (a) Schematic diagram and energy level diagram of the ST-OSC with an invented architecture of ITO/Al(acac)$_3$/PBDB-T-2F:Y6/MoO$_3$/Ag. (b) Schematic diagram of the OPV with the ultrathin ALD TiO$_x$ passivation layer. (c) Schematic diagram of a semitransparent device with the architecture of ITO/SnO$_2$/active layer/MoO$_3$/Ag and schematic energy level diagrams of device components referenced to the vacuum level; (d) Energy levels of ITO, PEDOT:PSS, PTB7-Th, PC$_{71}$BM, and PF3N-2TNDI. (e) Device architecture of Ag/Au alloy NP-induced semitransparent OPV. Reproduced (a) with permission from ref. [71], (b) with permission from ref. [72], (c) with permission from ref. [73], (d) with permission from ref. [74], and (e) with permission from ref. [75]. Copyright 2020 The Royal Society of Chemistry, 2020 Wiley-VCH, 2019 The Royal Society of Chemistry, 2017 Wiley-VCH, and 2018 American Chemical Society, respectively.

crystals could confer nearly optimal properties on semitransparent OPVs, which indicated that high-performance devices could be made with simple device architecture (Fig. 10a). Guided by computer simulations, they fabricated semitransparent OPVs with single-pair photo crystal and PTB7-Th:IEICO-4F as the active layer. The device exhibited nearly 11% PCE and 30% AVT. This systematic study of photo crystals on semitransparent OPV provided guideline of the optical engineering.

To utilize more photons in the NIR region, Forrest et al. combined an outcoupling (OC) layer with an antireflection coating (ARC) in the semitransparent devices (Fig. 10b) [64]. As a result, the AVT increased while the reflection in the NIR was also enhanced. This approach allowed the implementation of more materials into the device architecture without degrading the electrical characteristics. With this strategy, optimized devices with PCE of 8.0 ± 0.2% with AVT of 44.2 ± 1.4% were achieved. Meanwhile, the neutral semitransparent OPV showed PCE of 5.8 ± 0.2% with AVT of 44.3 ± 1.5%. When utilizing a distributed Bragg reflector (DBR) mirror on top of semitransparent contact, the PCE was further improved to 8.2 ± 0.3%.

Similarly, Hou et al. reported on a semitransparent OPV with blends with polymer and fullerene. It was sandwiched between a bottom one-dimensional photonic crystal (1DPC) and a top solution-processed highly conductive PEDOT:PSS electrode for light harvesting (Fig. 10c) [78]. They found that the active layer thickness hardly influenced the theoretical J_{SC} of 1DPC-STPSC due to the relatively weaker microcavity effect compared to that of the conventional opaque devices. It demonstrated a stronger microcavity effect compared to the non-microcavity devices, which was beneficial to both enhancing the light absorption in active blends in the strong absorption band and maintaining visible light transmittance in the weak absorption band. The PCE and J_{SC} of the devices increased by 37% and 38%, respectively, compared with those of the semitransparent OPVs without using 1DPC. Later in 2020, the same group employed a polymer flexible one-dimensional photonic crystal (F-1DPC) to the semitransparent devices [79]. Based on the reasonable optimization of electrical and optical characteristics in the device, the maximum PCE of the devices with polymer F-1DPC was greatly improved by 24–27% compared to the ones without F-1DPC. And the increase in J_{SC} was mainly ascribed to the enhancement of effective photon absorption in the device.

Shen et al. demonstrated a new kind of semitransparent OPVs by controlling the optical Tamm state (OTS) at the interface between thin Ag electrodes and extra added layer (EAL)/1DPCs (Fig. 10d) [80]. The transmittance groove of Ag/EAL/1DPCs was gradually redshifted and broadened by adjusting the position and intensity of the OTS. As a result, a PCE of 9.36% with an AVT of 14.31% was achieved. Simulations carried out by transfer matrix modeling (TMM) demonstrated that the photoelectric field

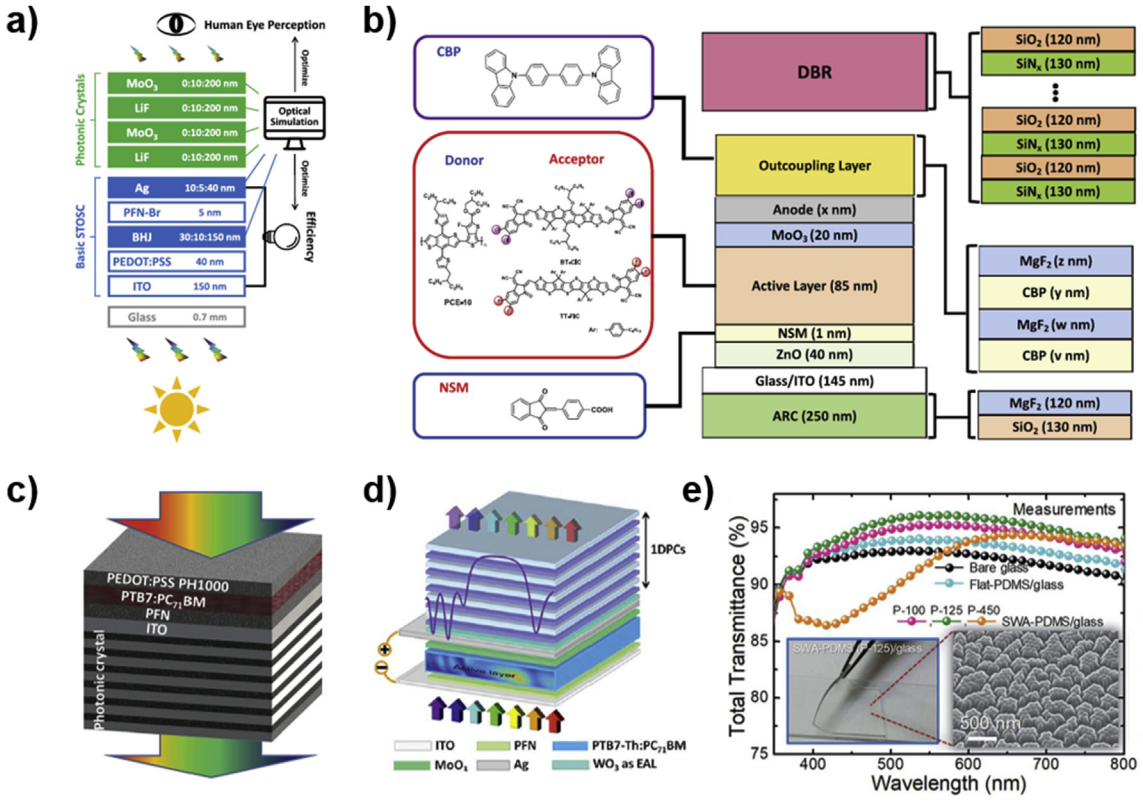

Fig. 10. Strategy of photonic reflector. (a) Device structure and layer thicknesses of PC-enhanced semitransparent OPVs. (b) Schematic of the semitransparent device showing optimized layer thicknesses and compositions. Left: molecular structural formulae of the NSM, CBP, donors (PCE-10), and acceptors (TT-FIC and BT-CIC). Right: detailed layer structures of the outcoupling layer, antireflection layer, and distributed Bragg reflector. (c) Schematic of the device structure of the device with bottom periodic one-dimensional photonic crystal. (d) The semitransparent OPV with the architecture ITO/PFN/PTB7-Th:$PC_{71}BM$/MoO_3/Ag/WO_3 (EAL)[WO_3/LiF] [5]. (e) Measured total transmittance spectra of bare glass, flat-PDMS, and SWA-PDMS layers with various periods (P-100, P-125, and P-450) laminated on the glass. Reproduced (a) with permission from ref. [77], (b) with permission from ref. [64], (c) with permission from ref. [78], (d) with permission from ref. [80], and (e) with permission from ref. [81]. Copyright 2019 Cell Press, 2019 Wiley-VCH, 2016 The Royal Society of Chemistry, 2019 The Royal Society of Chemistry, and 2018 The Royal Society of Chemistry, respectively.

intensity can be redistributed by controlling the OTS, resulting in an enhancement in the absorption of the devices.

Besides, Yu et al. reported semitransparent OPVs with subwavelength architectured polydimethylsiloxane (SWA-PDMS) as an antireflective (AR) layer on the glass substrate (Fig. 10e) [81]. The subwavelength architectures (SWAs) on PDMS layers were fabricated by a soft imprint lithography technique using an anodic aluminum oxide mold. By investigating the influence of optical characteristics of SWA-PDMS with respect to the period and diameter of SWAs, they found that the SWA-PDMS/glass with a period and diameter of 125 nm and 80 nm, respectively, was the optimal sample, exhibiting the highest average transmittance (T_{avg}) of 95.2%, which was much higher than that of bare glass (T_{avg} 92.08%). After applying the optimal SWA-PDMS on the glass surface of opaque and semitransparent OPVs as an AR layer, their PCEs were improved from 8.67% to 10.59% and 7.07% to 8.52%, respectively. Besides, the AVT of the semitransparent OPVs increased from 23.0% to 26.2% with significantly improved color coordinates when the AR layer was employed. The devices with SWA-PDMS also exhibited a high hydrophobic nature and a good stability in the ambient environment.

5. Conclusion and perspectives

Because of the tunable properties of the organic materials, semitransparent OPVs are quite suitable for the agricultural applications. When designing the semitransparent OPV devices for the agricultural applications, we need to consider the light wavelength for the plant photosynthesis instead of the visible range. Thus, in this review we specifically bring up the requirements of the devices for the greenhouses. Although most of the research on the semitransparent OPVs only focus on the transmittance at the visible wavelength range, we can still obtain valuable experiences for the agricultural application. The major enhancements of the semitransparent solar cells can be categorized into material design for active layers, development of the electrode, and structural modifications. Some of the strategies do not solve the basic contradiction between the PCE and AVT of the semitransparent devices, but they might be able to get utilized for specific requirements. For example, for the plants that do not need too much sun light while growing, we can increase the PCE of the devices to generate more electric power by scarifying the transmittance. Other powerful strategies, such as the application of ternary/quaternary systems, electrodes with higher transparency, and structural modification including the introduction of interlayers and the photo reflectors, should be synergistically applied into the semitransparent OPVs for further enhancement of the device performances and more suitable transmittance alignment of the photosynthesis.

As one of the most promising applications of the semitransparent OPVs, the photo-agricultural research is still facing challenges. Since the agricultural application requires continuous outdoor operation under different climate conditions, the major challenge that we need to resolve is the operational stability of the semitransparent devices. The ability against harsh environments such as high temperature and humidity will play an important role deciding the market size of the solar panel. This aspect of research

is also in lack in most of the state-of-art works. The second problem of the semitransparent OPVs for agricultural application is the dropped PCEs of the large-area devices. Considering the vast agricultural acreage in the remote area, large-area OPV devices with high performance and mild flexibility are needed. Hence, the development of novel active layers and electrodes with preferrable horizontal charge carrier transportation are in urgent demand. The third challenge of the semitransparent OPVs for agricultural application is the match of the absorption spectra of the devices and the plants beneath. Different from the works only focused on the enhancements of the AVTs and PCEs, the research on semitransparent OPVs for agricultural applications will be more effective to only consider the transmittance of the light that needed for the photosynthesis. This requires detailed design of the active layers and photonic reflectors of the semitransparent devices. Absorber molecules that avoid absorption in the photosynthetic region and novel reflectors that selectively allows the transmittance of specific light wavelength are expected in the future research.

Based on these, we should address those further developments of the active layer materials should be the key to semitransparent OPVs for agricultural applications. Rational design of stable donor/acceptor molecules with preferred transmittance spectra and ideal horizontal charge carrier transportation will greatly carry forward the commercialization of the semitransparent OPVs. Besides that, more advanced electrodes and structural modification could help us to obtain more favorable performances. In general, we believe that the semitransparent OPVs for the agricultural application holds a strong promise for the solar market and will significantly change the modern society. Additional evolutions are expected and hopefully we can bring this technology into the industry in the near future.

Declaration of competing interest

The authors declare that they have no known competing financial interests or personal relationships that could have appeared to influence the work reported in this paper.

Acknowledgments

This work was supported by the California Energy Commission (No. EPC-19-002).

References

[1] A. Wu, G.L. Hammer, A. Doherty, S. von Caemmerer, G.D. Farquhar, Quantifying impacts of enhancing photosynthesis on crop yield, Nat. Plants 5 (4) (2019) 380.
[2] A. Yano, M. Cossu, Energy sustainable greenhouse crop cultivation using photovoltaic technologies, Renew. Sust. Energy Rev. 109 (2019) 116.
[3] R. Waller, M. Kacira, E. Magadley, M. Teitel, I. Yehia, Semi-transparent organic photovoltaics applied as greenhouse shade for spring and summer tomato production in arid climate, Agronomy 11 (6) (2021) 1152.
[4] H. Shi, R. Xia, G. Zhang, H.L. Yip, Y. Cao, Spectral engineering of semitransparent polymer solar cells for greenhouse applications, Adv. Energy Mater. 9 (5) (2019) 1803438.
[5] F. Yang, Y. Zhang, Y. Hao, Y. Cui, W. Wang, T. Ji, F. Shi, B. Wei, Visibly transparent organic photovoltaic with improved transparency and absorption based on tandem photonic crystal for greenhouse application, Appl. Opt. 54 (34) (2015) 10232.
[6] Y. Akhmetov, M. Bagheri, G. Gharehpetian, Modeling and analysis of a renewable-energy-powered greenhouse, in: 2019 International Aegean Conference on Electrical Machines and Power Electronics (ACEMP) & 2019 International Conference on Optimization of Electrical and Electronic Equipment (OPTIM), IEEE, 2019, p. 506.
[7] P.V. Nelson, Greenhouse Operation and Management, Prentice-Hall, 1991.
[8] L. La Notte, L. Giordano, E. Calabrò, R. Bedini, G. Colla, G. Puglisi, A. Reale, Hybrid and organic photovoltaics for greenhouse applications, Appl. Energy 278 (2020) 115582.
[9] S. Gorjian, H. Ebadi, G. Najafi, S.S. Chandel, H. Yildizhan, Recent advances in net-zero energy greenhouses and adapted thermal energy storage systems, Sustain. Energy Technol. Assess. 43 (2021) 100940.
[10] H.C. Kim, V. Fthenakis, J.K. Choi, D.E. Turney, Life cycle greenhouse gas emissions of thin-film photovoltaic electricity generation: systematic review and harmonization, J. Ind. Ecol. 16 (2012) S110.
[11] J.D. Bergesen, G.A. Heath, T. Gibon, S. Suh, Thin-film photovoltaic power generation offers decreasing greenhouse gas emissions and increasing environmental co-benefits in the long term, Environ. Sci. Technol. 48 (16) (2014) 9834.
[12] D.D. Hsu, P. O'Donoughue, V. Fthenakis, G.A. Heath, H.C. Kim, P. Sawyer, J.K. Choi, D.E. Turney, Life cycle greenhouse gas emissions of crystalline silicon photovoltaic electricity generation: systematic review and harmonization, J. Ind. Ecol. 16 (2012) S122.
[13] R. Kommalapati, A. Kadiyala, M. Shahriar, Z. Huque, Review of the life cycle greenhouse gas emissions from different photovoltaic and concentrating solar power electricity generation systems, Energies 10 (3) (2017) 350.
[14] F. Cucchiella, I. D'Adamo, Estimation of the energetic and environmental impacts of a roof-mounted building-integrated photovoltaic systems, Renew. Sust. Energy Rev. 16 (7) (2012) 5245.
[15] N.A. Ludin, N.I. Mustafa, M.M. Hanafiah, M.A. Ibrahim, M.A.M. Teridi, S. Sepeai, A. Zaharim, K. Sopian, Prospects of life cycle assessment of renewable energy from solar photovoltaic technologies: a review, Renew. Sust. Energy Rev. 96 (2018) 11.
[16] M.F. Peretz, F. Geoola, I. Yehia, S. Ozer, A. Levi, E. Magadley, R. Brikman, L. Rosenfeld, A. Levy, M. Kacira, Testing organic photovoltaic modules for application as greenhouse cover or shading element, Biosyst. Eng. 184 (2019) 24.
[17] C.S. Allardyce, C. Fankhauser, S.M. Zakeeruddin, M. Grätzel, P.J. Dyson, The influence of greenhouse-integrated photovoltaics on crop production, Sol. Energy 155 (2017) 517.
[18] C.J. Emmott, J.A. Röhr, M. Campoy-Quiles, T. Kirchartz, A. Urbina, N.J. Ekins-Daukes, J. Nelson, Organic photovoltaic greenhouses: a unique application for semi-transparent PV? Energy Environ. Sci. 8 (4) (2015) 1317.
[19] C. Li, J. Zhou, J. Song, J. Xu, H. Zhang, X. Zhang, J. Guo, L. Zhu, D. Wei, G. Han, Non-fullerene acceptors with branched side chains and improved molecular packing to exceed 18% efficiency in organic solar cells, Nat. Energy 6 (6) (2021) 605.
[20] F. Liu, L. Zhou, W. Liu, Z. Zhou, Q. Yue, W. Zheng, R. Sun, W. Liu, S. Xu, H. Fan, Organic solar cells with 18% efficiency enabled by an alloy acceptor: a two-in-one strategy, Adv. Mater. (2021) 2100830.
[21] Y. Cui, H. Yao, J. Zhang, K. Xian, T. Zhang, L. Hong, Y. Wang, Y. Xu, K. Ma, C. An, Single-junction organic photovoltaic cells with approaching 18% efficiency, Adv. Mater. 32 (19) (2020) 1908205.
[22] W. Chen, Q. Zhang, Recent progress in non-fullerene small molecule acceptors in organic solar cells (OSCs), J. Mater. Chem. C 5 (6) (2017) 1275.
[23] H. Sun, X. Song, J. Xie, P. Sun, P. Gu, C. Liu, F. Chen, Q. Zhang, Z.-K. Chen, W. Huang, PDI derivative through fine-tuning the molecular structure for fullerene-free organic solar cells, ACS Appl. Mater. Interfaces 9 (35) (2017) 29924.
[24] W. Chen, X. Yang, G. Long, X. Wan, Y. Chen, Q. Zhang, A perylene diimide (PDI)-based small molecule with tetrahedral configuration as a non-fullerene acceptor for organic solar cells, J. Mater. Chem. C 3 (18) (2015) 4698.
[25] R. Sun, Q. Wu, J. Guo, T. Wang, Y. Wu, B. Qiu, Z. Luo, W. Yang, Z. Hu, J. Guo, A layer-by-layer architecture for printable organic solar cells overcoming the scaling lag of module efficiency, Joule 4 (2) (2020) 407.
[26] M. Riede, D. Spoltore, K. Leo, Organic solar cells—the path to commercial success, Adv. Energy Mater. 11 (1) (2021) 2002653.
[27] K. Inada, Action spectra for photosynthesis in higher plants, Plant Cell Physiol. 17 (2) (1976) 355.
[28] C. Stanghellini, J. Dai, F. Kempkes, Effect of near-infrared-radiation reflective screen materials on ventilation requirement, crop transpiration and water use efficiency of a greenhouse rose crop, Biosyst. Eng. 110 (3) (2011) 261.
[29] E. Ravishankar, R.E. Booth, C. Saravitz, H. Sederoff, H.W. Ade, B.T. O'Connor, Achieving net zero energy greenhouses by integrating semitransparent organic solar cells, Joule 4 (2) (2020) 490.
[30] C. Baxevanou, D. Fidaros, N. Katsoulas, E. Mekeridis, C. Varlamis, A. Zachariadis, S. Logothetidis, Simulation of radiation and crop activity in a greenhouse covered with semitransparent organic photovoltaics, Appl. Sci. 10 (7) (2020) 2550.
[31] Y. Tang, X. Ma, M. Li, Y. Wang, The effect of temperature and light on strawberry production in a solar greenhouse, Sol. Energy 195 (2020) 318.
[32] D. Wang, R. Qin, G. Zhou, X. Li, R. Xia, Y. Li, L. Zhan, H. Zhu, X. Lu, H.L. Yip, High-performance semitransparent organic solar cells with excellent infrared reflection and see-through functions, Adv. Mater. 32 (32) (2020) 2001621.
[33] T. Xiao, J. Wang, S. Yang, Y. Zhu, D. Li, Z. Wang, S. Feng, L. Bu, X. Zhan, G. Lu, Film-depth-dependent crystallinity for light transmission and charge transport in semitransparent organic solar cells, J. Mater. Chem. A 8 (1) (2020) 401.
[34] X. Ma, Z. Xiao, Q. An, M. Zhang, Z. Hu, J. Wang, L. Ding, F. Zhang, Simultaneously improved efficiency and average visible transmittance of semitransparent polymer solar cells with two ultra-narrow bandgap nonfullerene acceptors, J. Mater. Chem. A 6 (43) (2018) 21485.
[35] Y. Li, X. Guo, Z. Peng, B. Qu, H. Yan, H. Ade, M. Zhang, S.R. Forrest, Color-neutral, semitransparent organic photovoltaics for power window applications, Proc. Natl. Acad. Sci. 117 (35) (2020) 21147.

[36] Y. Cui, C. Yang, H. Yao, J. Zhu, Y. Wang, G. Jia, F. Gao, J. Hou, Efficient semitransparent organic solar cells with tunable color enabled by an ultralow bandgap nonfullerene acceptor, Adv. Mater. 29 (43) (2017) 1703080.
[37] Z. Hu, Z. Wang, F. Zhang, Semitransparent polymer solar cells with 9.06% efficiency and 27.1% average visible transmittance obtained by employing a smart strategy, J. Mater. Chem. A 7 (12) (2019) 7025.
[38] Y. Xie, Y. Cai, L. Zhu, R. Xia, L. Ye, X. Feng, H.L. Yip, F. Liu, G. Lu, S. Tan, Fibril network strategy enables high-performance semitransparent organic solar cells, Adv. Funct. Mater. 30 (28) (2020) 2002181.
[39] Z. Hu, J. Wang, X. Ma, J. Gao, C. Xu, X. Wang, X. Zhang, Z. Wang, F. Zhang, Semitransparent organic solar cells exhibiting 13.02% efficiency and 20.2% average visible transmittance, J. Mater. Chem. A 9 (11) (2021) 6797.
[40] L. Duan, H. Yi, Z. Wang, Y. Zhang, F. Haque, B. Sang, R. Deng, A. Uddin, Semitransparent organic solar cells based on PffBT4T-2OD with a thick active layer and near neutral colour perception for window applications, Sustain. Energy Fuels 3 (9) (2019) 2456.
[41] M.M. Tavakoli, R. Po, G. Bianchi, A. Cominetti, C. Carbonera, N. Camaioni, F. Tinti, J. Kong, A relatively wide-bandgap and air-stable donor polymer for fabrication of efficient semitransparent and tandem organic photovoltaics, Proc. Natl. Acad. Sci. 116 (44) (2019) 22037.
[42] X. Huang, J. Oh, Y. Cheng, B. Huang, S. Ding, Q. He, F. Wu, C. Yang, L. Chen, Y. Chen, Narrow band-gap materials with overlapping absorption simultaneously increase the open circuit voltage and average visible transmittance of semitransparent organic solar cells, J. Mater. Chem. A 9 (9) (2021) 5711.
[43] Z. Hu, J. Wang, Z. Wang, W. Gao, Q. An, M. Zhang, X. Ma, J. Wang, J. Miao, C. Yang, Semitransparent ternary nonfullerene polymer solar cells exhibiting 9.40% efficiency and 24.6% average visible transmittance, Nano Energy 55 (2019) 424.
[44] N.G. An, T. Lee, J. Heo, J.W. Kim, S. Song, W. Lee, B. Walker, E. Lim, J.Y. Kim, Exploiting ternary blends to accurately control the coloration of semitransparent, non-fullerene, organic solar cells, Sol. RRL 5 (3) (2021) 2000742.
[45] Y. Xie, L. Huo, B. Fan, H. Fu, Y. Cai, L. Zhang, Z. Li, Y. Wang, W. Ma, Y. Chen, High-performance semitransparent ternary organic solar cells, Adv. Funct. Mater. 28 (49) (2018) 1800627.
[46] P. Yin, Z. Yin, Y. Ma, Q. Zheng, Improving the charge transport of the ternary blend active layer for efficient semitransparent organic solar cells, Energy Environ. Sci. 13 (12) (2020) 5177.
[47] X. Lu, L. Cao, X. Du, H. Lin, C. Zheng, Z. Chen, B. Sun, S. Tao, Hydrogen-bond-induced high performance semitransparent ternary organic solar cells with 14% efficiency and enhanced stability, Adv. Opt. Mater. (2021) 2100064.
[48] M. Nam, H.Y. Noh, J.-H. Kang, J. Cho, B.K. Min, J.W. Shim, D.-H. Ko, Semitransparent quaternary organic blends for advanced photovoltaic applications, Nano Energy 58 (2019) 652.
[49] Y. Cho, T.H. Lee, S. Jeong, S.Y. Park, B. Lee, J.Y. Kim, C. Yang, Dithienogermole-based nonfullerene acceptors: roles of the side-chains' direction and development of green-tinted efficient semitransparent organic solar cells, ACS Appl. Energy Mater. 3 (8) (2020) 7689.
[50] X. Du, X. Li, H. Lin, L. Zhou, C. Zheng, S. Tao, High performance opaque and semi-transparent organic solar cells with good tolerance to film thickness realized by a unique solid additive, J. Mater. Chem. A 7 (13) (2019) 7437.
[51] Y. Liu, Y. Yan, Q. Zhang, J. Zhang, X. Yu, Y. Han, Increasing the nucleation and growth barrier of a non-fullerene acceptor to achieve bicontinuous pathways in semitransparent ternary polymer solar cells, J. Mater. Chem. C 9 (17) (2021) 5713.
[52] H.C. Wang, P. Cheng, S. Tan, C.H. Chen, B. Chang, C.S. Tsao, L.Y. Chen, C.A. Hsieh, Y.C. Lin, H.W. Cheng, Sequential deposition of donor and acceptor provides high-performance semitransparent organic photovoltaics having a pseudo p–i–n active layer structure, Adv. Energy Mater. 11 (13) (2021) 2003576.
[53] http://www.ledgrowlightshq.co.uk/chlorophyll-plant-pigments/.
[54] D. Wang, H. Liu, Y. Li, G. Zhou, L. Zhan, H. Zhu, X. Lu, H. Chen, C.-Z. Li, High-performance and eco-friendly semitransparent organic solar cells for greenhouse applications, Joule 5 (4) (2021) 945.
[55] Y. Kim, J. Son, S. Shafian, K. Kim, J.K. Hyun, Semitransparent blue, green, and red organic solar cells using color filtering electrodes, Adv. Opt. Mater. 6 (13) (2018) 1800051.
[56] S. Shafian, J. Son, Y. Kim, J.K. Hyun, K. Kim, Active-material-independent color-tunable semitransparent organic solar cells, ACS Appl. Mater. Interfaces 11 (21) (2019) 18887.
[57] S. Wang, J. Chen, L. Li, L. Zuo, T.-Y. Qu, H. Ren, Y. Li, A.K.-Y. Jen, J.-X. Tang, Narrow bandpass and efficient semitransparent organic solar cells based on bioinspired spectrally selective electrodes, ACS Nano 14 (5) (2020) 5998.
[58] S.K. Hau, H.-L. Yip, J. Zou, A.K.-Y. Jen, Indium tin oxide-free semi-transparent inverted polymer solar cells using conducting polymer as both bottom and top electrodes, Org. Electron. 10 (7) (2009) 1401.
[59] Y. Wang, B. Jia, F. Qin, Y. Wu, W. Meng, S. Dai, Y. Zhou, X. Zhan, Semitransparent, non-fullerene and flexible all-plastic solar cells, Polymer 107 (2016) 108.
[60] W. Song, B. Fanady, R. Peng, L. Hong, L. Wu, W. Zhang, T. Yan, T. Wu, S. Chen, Z. Ge, Foldable semitransparent organic solar cells for photovoltaic and photosynthesis, Adv. Energy Mater. 10 (15) (2020) 2000136.
[61] B. O'Connor, C. Haughn, K.-H. An, K.P. Pipe, M. Shtein, Transparent and conductive electrodes based on unpatterned, thin metal films, Appl. Phys. Lett. 93 (22) (2008) 433.
[62] S. Schubert, J. Meiss, L. Müller-Meskamp, K. Leo, Improvement of transparent metal top electrodes for organic solar cells by introducing a high surface energy seed layer, Adv. Energy Mater. 3 (4) (2013) 438.
[63] D.S. Ghosh, Q. Liu, P. Mantilla-Perez, T.L. Chen, V. Mkhitaryan, M. Huang, S. Garner, J. Martorell, V. Pruneri, Highly flexible transparent electrodes containing ultrathin silver for efficient polymer solar cells, Adv. Funct. Mater. 25 (47) (2015) 7309.
[64] Y. Li, C. Ji, Y. Qu, X. Huang, S. Hou, C.Z. Li, L.S. Liao, L.J. Guo, S.R. Forrest, Enhanced light utilization in semitransparent organic photovoltaics using an optical outcoupling architecture, Adv. Mater. 31 (40) (2019) 1903173.
[65] J. Krantz, T. Stubhan, M. Richter, S. Spallek, I. Litzov, G.J. Matt, E. Spiecker, C.J. Brabec, Spray-coated silver nanowires as top electrode layer in semitransparent P3HT: PCBM-based organic solar cell devices, Adv. Funct. Mater. 23 (13) (2013) 1711.
[66] H. Lu, J. Lin, N. Wu, S. Nie, Q. Luo, C.-Q. Ma, Z. Cui, Inkjet printed silver nanowire network as top electrode for semi-transparent organic photovoltaic devices, Appl. Phys. Lett. 106 (9) (2015) 27_1.
[67] W. Gaynor, J.-Y. Lee, P. Peumans, Fully solution-processed inverted polymer solar cells with laminated nanowire electrodes, ACS Nano 4 (1) (2010) 30.
[68] J.-Y. Lee, S.T. Connor, Y. Cui, P. Peumans, Semitransparent organic photovoltaic cells with laminated top electrode, Nano Lett. 10 (4) (2010) 1276.
[69] C.-C. Chen, L. Dou, R. Zhu, C.-H. Chung, T.-B. Song, Y.B. Zheng, S. Hawks, G. Li, P.S. Weiss, Y. Yang, Visibly transparent polymer solar cells produced by solution processing, ACS Nano 6 (8) (2012) 7185.
[70] P. Maisch, K.C. Tam, L. Lucera, H.-J. Egelhaaf, H. Scheiber, E. Maier, C.J. Brabec, Inkjet printed silver nanowire percolation networks as electrodes for highly efficient semitransparent organic solar cells, Org. Electron. 38 (2016) 139.
[71] Y. Bai, C. Zhao, R. Shi, J. Wang, F. Wang, T. Hayat, A. Alsaedi, Z.a. Tan, Novel cathode buffer layer of Al (acac) 3 enables efficient, large area and stable semitransparent organic solar cells, Mater. Chem. Front. 4 (7) (2020) 2072.
[72] L. Duan, B. Sang, M. He, Y. Zhang, M.A. Hossain, M.H. Rahaman, Q. Wei, Y. Zou, A. Uddin, B. Hoex, Interface modification enabled by atomic layer deposited ultra-thin titanium oxide for high-efficiency and semitransparent organic solar cells, Sol. RRL 4 (12) (2020) 2000497.
[73] Y. Bai, C. Zhao, X. Chen, S. Zhang, S. Zhang, T. Hayat, A. Alsaedi, Z.a. Tan, J. Hou, Y. Li, Interfacial engineering and optical coupling for multicolored semitransparent inverted organic photovoltaics with a record efficiency of over 12%, J. Mater. Chem. A 7 (26) (2019) 15887.
[74] H. Shi, R. Xia, C. Sun, J. Xiao, Z. Wu, F. Huang, H.L. Yip, Y. Cao, Synergic interface and optical engineering for high-performance semitransparent polymer solar cells, Adv. Energy Mater. 7 (20) (2017) 1701121.
[75] P. Shen, G. Wang, B. Kang, W. Guo, L. Shen, High-efficiency and high-color-rendering-index semitransparent polymer solar cells induced by photonic crystals and surface plasmon resonance, ACS Appl. Mater. Interfaces 10 (7) (2018) 6513.
[76] Y. Li, C. He, L. Zuo, F. Zhao, L. Zhan, X. Li, R. Xia, H.L. Yip, C.Z. Li, X. Liu, H.Z. Chen, High-performance semi-transparent organic photovoltaic devices via improving absorbing selectivity, Adv. Energy Mater. 11 (11) (2021) 2003408.
[77] R. Xia, C.J. Brabec, H.-L. Yip, Y. Cao, High-throughput optical screening for efficient semitransparent organic solar cells, Joule 3 (9) (2019) 2241.
[78] Y. Zhang, Z. Peng, C. Cai, Z. Liu, Y. Lin, W. Zheng, J. Yang, L. Hou, Y. Cao, Colorful semitransparent polymer solar cells employing a bottom periodic one-dimensional photonic crystal and a top conductive PEDOT: PSS layer, J. Mater. Chem. A 4 (30) (2016) 11821.
[79] W. Zheng, X. Luo, Y. Zhang, C. Ye, A. Qin, Y. Cao, L. Hou, Efficient low-cost all-flexible microcavity semitransparent polymer solar cells enabled by polymer flexible one-dimensional photonic crystals, ACS Appl. Mater. Interfaces 12 (20) (2020) 23190.
[80] P. Shen, M. Yao, J. Liu, Y. Long, W. Guo, L. Shen, Colored semitransparent polymer solar cells with a power conversion efficiency of 9.36% achieved by controlling the optical Tamm state, J. Mater. Chem. A 7 (8) (2019) 4102.
[81] B. Dudem, J.W. Jung, J.S. Yu, Improved light harvesting efficiency of semitransparent organic solar cells enabled by broadband/omnidirectional subwavelength antireflective architectures, J. Mater. Chem. A 6 (30) (2018) 14769.